CHAPTER 6

PETROGRAPHY

6.1. GENERAL

From the metamorphic point of view, the rocks of the study area are quite interesting. Quartzites, chlorite schists, mica schists and calc-schists are the major rock types encountered in the area. The quartzites have formed by metamorphism of sandstones (psamites) whereas the chlorite schists and mica schists are a result of metamorphism of sedimentary rocks such as shales and greywacke (pelites). The transitional varieties i.e., psamites with increasing pelitic content have formed micaceous quartzites or quartzose mica schists. The deposits also contained some calcareous sediments sporadically, and these are seen today as calc-schist lensoid bands intercalated with mica schists and quartzites; these typically consist calc-silicate minerals like zoisite and actinolite. On the basis of study of several thin sections of metapelites from different parts of the study area the author has prepared a metamorphic grade map (Fig. 6.1) which shows the variation in the grade of metamorphism in the Lunavada region. Accordingly, it is observed that the rocks in sub-region-I (terminology as described in Chapters 3 & 4) are chlorite schists. No biotite is present in these rocks. The metapelites occupying sub-region-II (central parts of the study area) are generally biotite schists while those occurring in sub-region-III (southern parts of the study area) dominantly comprise garnet biotite schists. This clearly documents that the grade of metamorphism increases from N to

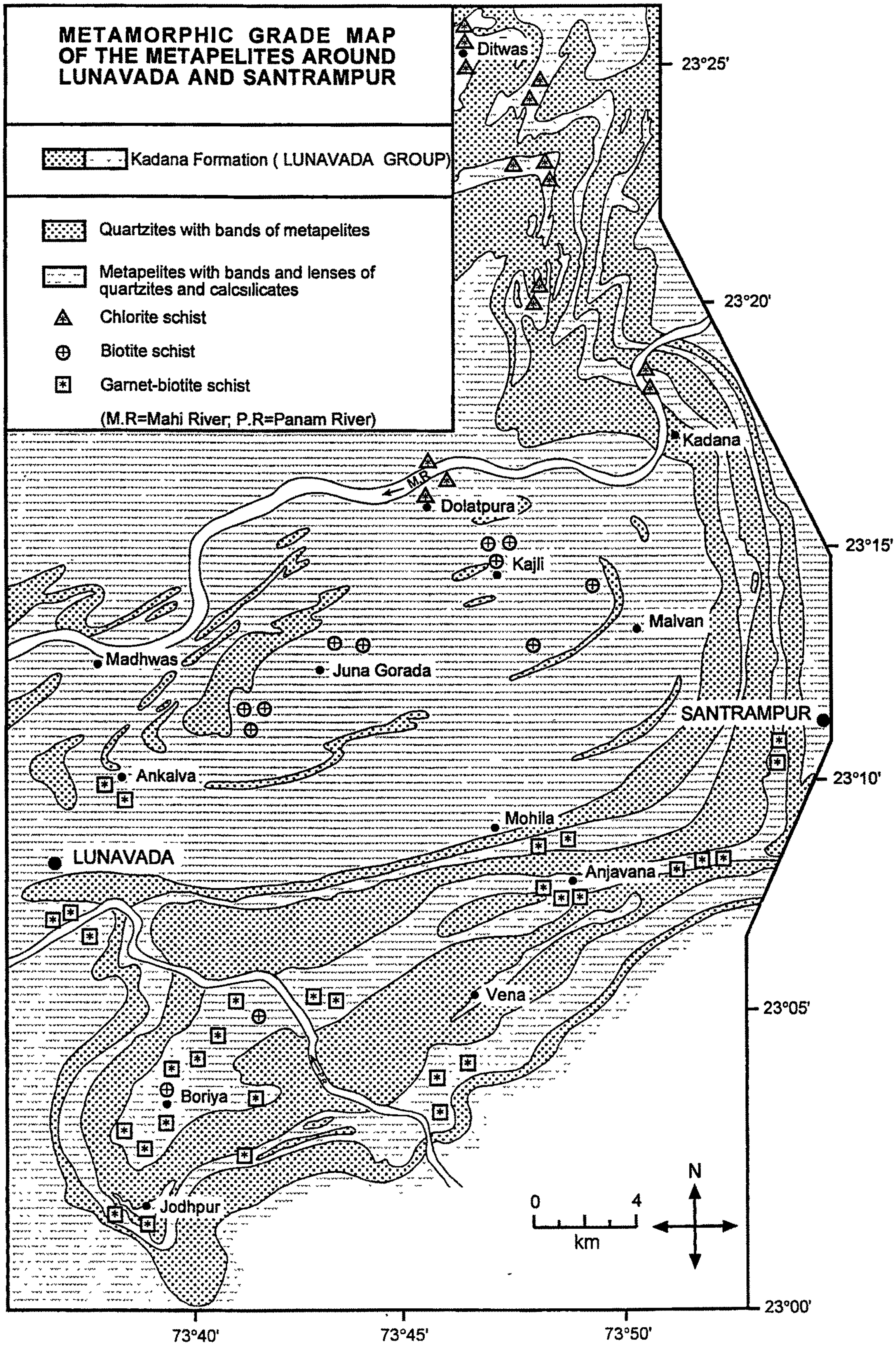
METAMORPHIC GRADE MAP OF THE METAPELITES AROUND LUNAVADA AND SANTRAMPUR
Kadana Formation (LUNAVADA GROUP)
Quartzites with bands of metapelites
Metapelites with bands and lenses of quartzites and calcsilicates
Chlorite schist
Biotite schist
Garnet-biotite schist
(M.R=Mahi River; P.R=Panam River)
Ditwas
Kadana
M.R
Dolatpura
Kajli
Malvan
Madhwas
Juna Gorada
SANTRAMPUR
Ankalva
Mohila
LUNAVADA
Anjavana
Vena
Boriya
Jodhpur
N
0
4
km
23°25'
23°20'
23°15'
23°10'
23°05'
23°00'
73°40'
73°45'
73°50'

S in the Lunavada region. This also implies that the southern parts of the study area represent deeper crustal levels.

The author has been able to identify minerals of more than one generation with the help of indepth petrographic and microstructural studies of the rocks, especially metapelites. It has also been possible for him to establish a correlation between their crystallization and deformational episodes. Table 6.1 is a list of mineral assemblages recognized by the author in different rock types of the study area.

As mentioned above, the study area comprises of five main rocks - quartzites, chlorite schists, biotite schists, garnet biotite schists and calc-schists. In the following pages of this chapter the author has given a detailed account of the mineral paragenesis in various rock types, their textural and petrographic characteristics and has worked out the correlation between metamorphic and deformational events.

6.2. CHLORITE SCHISTS

The chlorite schists are restricted in occurrence to the area N of Kadana-Dolatpura line (i.e. Sub-region-I described in chapters 3 and 4). Chlorite, muscovite and quartz are the dominant minerals. Three foliations S_0, S_1 and S_2 are recognisable on the microscale (Figs. 6.2, 6.3). The rocks have preserved primary lithological layering which is easily marked by alternating layers of quartz-rich and phyllosilicate rich layers (Figs. 6.2, 6.3). The alternation of layers rich and poor in phyllosilicates defines the original sedimentary bedding S_0. The S_1 foliation is sub-

Table 6.1.
Mineral assemblages in different rocks of the study area

Type of Sediment	Metamorphic equivalent	Mineral Assemblages
Pelites	Chlorite schist	chlotrite, muscovite and quartz
	Biotite schist	biotite, muscovite chlorite and quartz
	Garnet biotite schist	garnet, biotite, chlorite muscovite and quartz
Semi-pelite	Micaceous quartzite	quartz and muscovite
Psamite	Quartzite	quartz
Calcareous	Calc-schist	actinolite, zoisite, calcite, garnet, chlorite, sphene and quartz

parallel to S_0 and comprises parallely aligned chlorite, quartz and muscovite crystals. The third foliation is a discrete crenulation cleavage, S_2 which is formed on account of crenulation of S_1 foliation. The S_2 has developed almost perpendicular or at high angles to the S_1 and is observed to have formed only in the phyllosilicate rich layers. No significant metamorphism and formation of new minerals appears to have occurred along S_2 excepting recrystallized chlorite and muscovite crystals. Only one single generation of chlorite is prominent which occurs along S_1 foliation and has rotated and recrystallized into parallelism with S_2 during S_2 development. The paragenesis observed in the chlorite schists is *chlorite + muscovite + quartz* which is typical of chlorite zone and greenschist facies (Yardley, 1989; Spear, 1993).

Obviously the region to the N of Kadana has undergone one main episode of regional metamorphism related to the development of S_1 foliation during D_1 deformation. The S_2 foliation which is a discrete crenulation cleavage formed during D_2 deformation. No significant metamorphism appears to have occurred during D_2. However, some movement along the crenulation cleavage planes appears to have resulted in granulation and dislocation.

Discrete crenulation cleavage is the most prominent microstructure of the chlorite schists. As stated above, it has developed exclusively in the phyllosilicate-rich layers (Fig. 6.2, 6.3). There are evidences of displacement along the S_2 surface (Fig. 6.3). Similar apparent displacements in metapelites have been interpreted by Gray (1979) to be on account of pressure solution. However, at the present scale of observation, no significant evidence of recrystallized quartz aggregates and no metamorphic differentiation in the vicinity of the discrete crenulation cleavages along

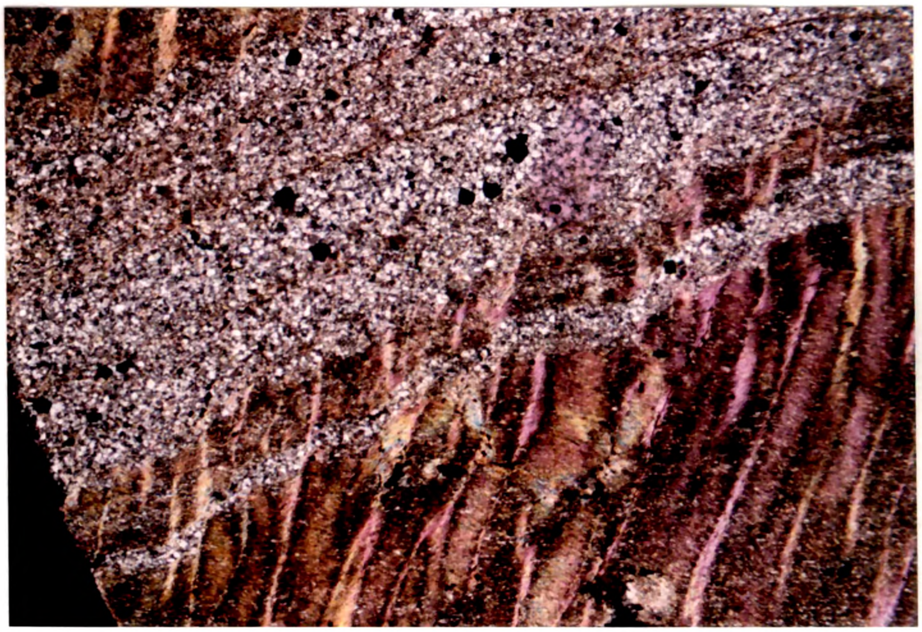

0.4 mm

Fig. 6.2 Photomicrograph of chlorite schist showing presence of S_0, S_1 and S_2 on the microscale. The bedding plane (S_0) is defined by the contact between quartz-rich and quartz-poor layers. The schistosity S_1 is sub-parallel to S_0 and is marked by chlorite and muscovite. The schistosity S_2 is a discrete crenulation cleavage which has developed at high angles to S_0 and S_1. The occurrence of the discrete crenulation cleavage is restricted to the quartz-poor (phyllosilicate-rich) layers. (X-nicols).

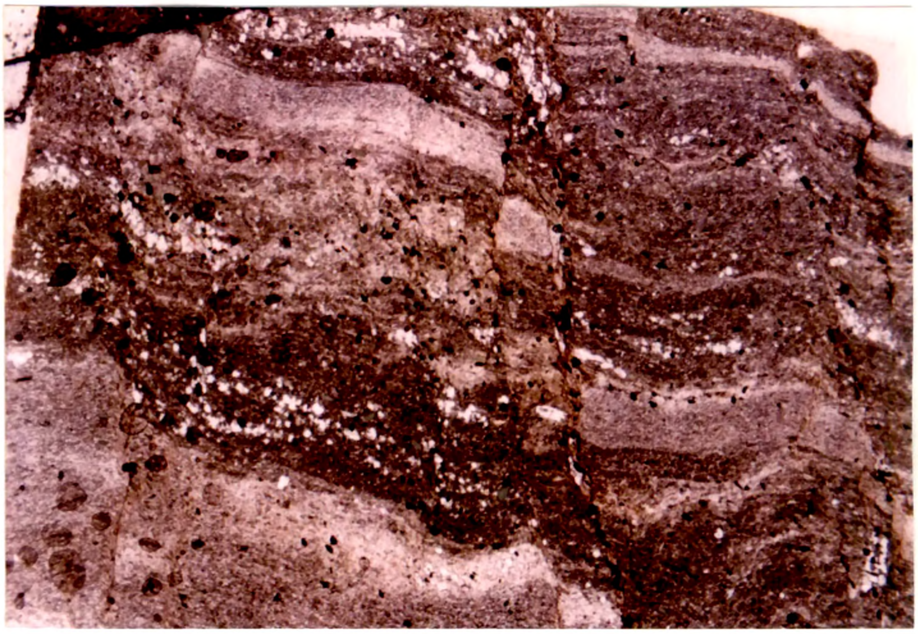

0.4 mm

Fig. 6.3. Photomicrograph of chlorite schist showing microscale displacement along the discrete crenulation cleavage (S_2). (PPL)

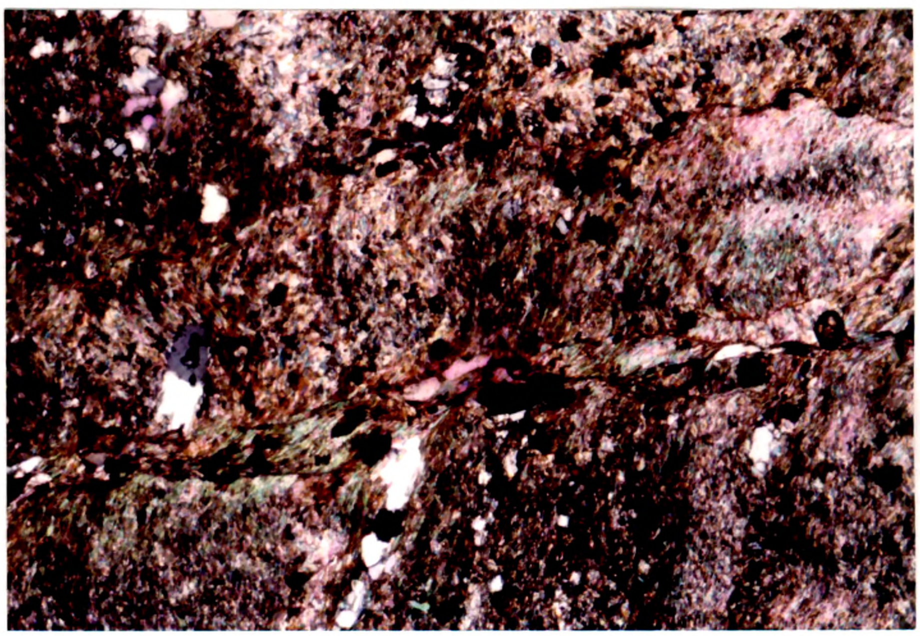

0.1 mm

Fig. 6.4. Photomicrograph documenting the drag effect along discrete crenulation cleavage (S_2) in chlorite schist. The S_1 foliation defined by muscovite and chlorite is observed to have dragged due to movement along the cleavage. (X-nicols).

which the apparent displacement occurred has been observed. Moreover, Fig. 6.4 shows some microscale dragging along the cleavages. Therefore the possibility of these crenulation cleavages being planes of shear cannot be totally ruled out. The chlorite schists possessing the discrete crenulation cleavages occur exclusively around Kadana and to its north and northwest along the Kadana-Dolatpura line. The crenulation cleavages are definitely on account of D_2 deformation. However, the displacement observed along the discrete crenulation cleavages could have occurred during D_3 deformation or during the later stages of the D_2 deformation. The fact that crenulation cleavages can behave as microscale shear zones has been documented in section 6.6.

6.3. MICA SCHIST

The central and southern parts of the study area (sub-regions II and III, chapter 3 & 4) comprise biotite schists and garnet-biotite schists respectively. Microstructures and textures observed in both the rock types are similar except for the presence of garnet in the garnet-biotite schists and their absence in the biotite schists. Therefore, the present section gives a detailed description largely of garnet-biotite schists. It is implied that similar microstructures also occur in the biotite schists.

The major minerals in biotite schists comprising sub-region-II are biotite, muscovite, chlorite and quartz. These mica schists often show more than one foliation and contain minerals of more than one generation. Three distinct foliations viz. S_0, S_1 and S_2 are preserved. S_0 is the primary lithological layering and is identified as the contact between a phyllosilicate rich layer and phyllosilicate poor layer. The quartz rich layers possess larger crystals of biotite and chlorite. The phyllosilicate rich layer is rich in chlorite, biotite and muscovite. The second foliation is the schistosity S_1 which is slightly oblique to S_0 (Fig. 6.5). The S_1 schistosity is defined by chlorite, muscovite and biotite flakes growing preferentially and parallel to each other, but oblique to the S_0. The third foliation is the S_2 schistosity, a crenulation cleavage. It marks microfolding or crenulation of S_1 schistosity and has developed at high angles to S_1 and S_0 at the hinge zone of F_2 folds.

S1 is oblique to S0 where parallel an part in Area I Can it be due to uneven deformation in single grain due to

The two foliations S_1 and S_2 are prominently developed in the garnet biotite schists of Sub-region-III (i.e. the region lying to the S of Lunavada and Santrampur tract). The primary lithological layering (S_0) i.e. the bedding is more or less totally obliterated in the schists of this area. The S_1 foliation has microfolded to form the S_2 foliation which is a differentiated crenulation cleavage (Fig. 6.6). Fine flakes of chlorite, muscovite, biotite and grains of quartz are the main minerals crystallizing along the microfolded S_1 foliation while large crystals of biotite, muscovite, some chlorite and quartz mark the S_2 foliation. Garnet is always present as porphyroblasts and often occurs in contact with biotite (Figs. 6.7, 6.8). Moreover, a few opaque minerals (ilmenite; see microprobe analysis in chapter 7) are present in the garnet porphyroblasts and also outside it.

Prograde Met?

Biotite and chlorite of more than one generation have been recognized on the basis of their preferred trends in the garnet biotite schists. The chlorite and biotite crystals occurring along S_1 are designated as chlorite(1) and biotite(1) respectively. Biotite crystals occurring along S_2 are referred to as biotite(2). The schists also

Is it valid?

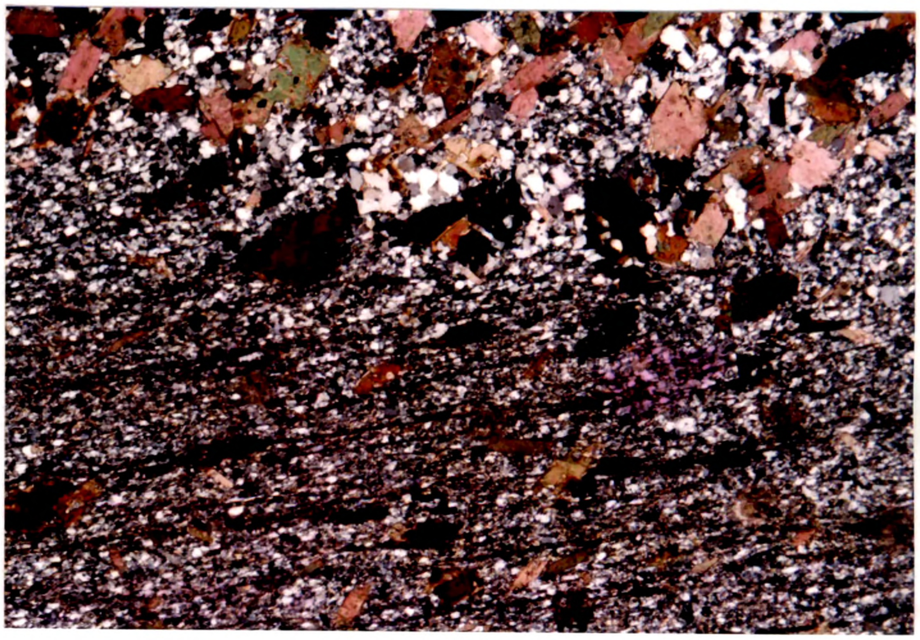

0.4 mm

Fig. 6.5. Photomicrograph showing oblique relationship between bedding (S_0) and cleavage (S_1) in biotite schist. The contact between the quartz rich and mica rich layers is the bedding plane. (X-nicols)

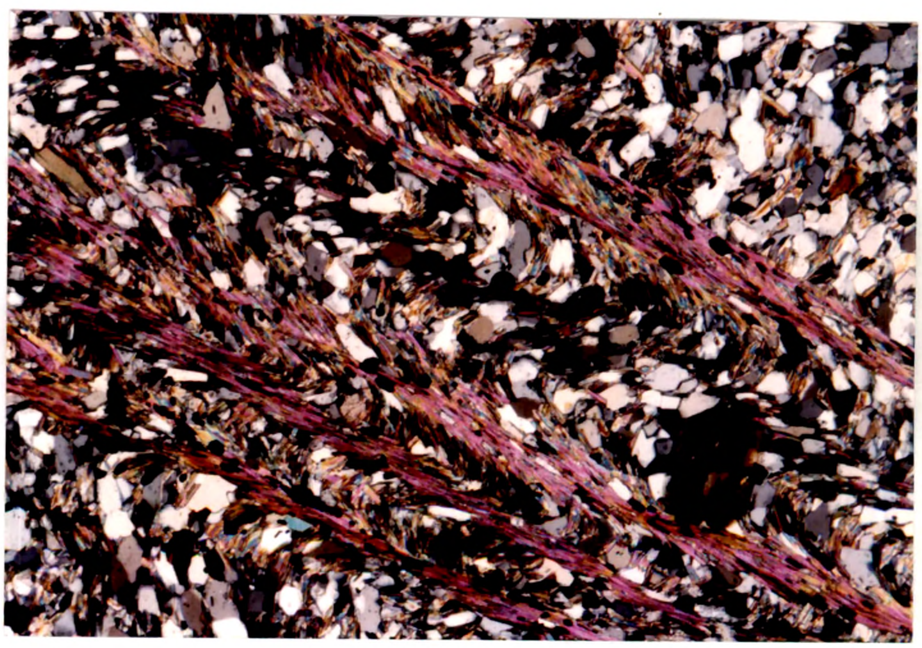

0.4 mm

Fig. 6.6. Photomicrograph exhibiting the presence of differentiated crenulation cleavage (S_2) in garnet biotite schist. (X-nicols).

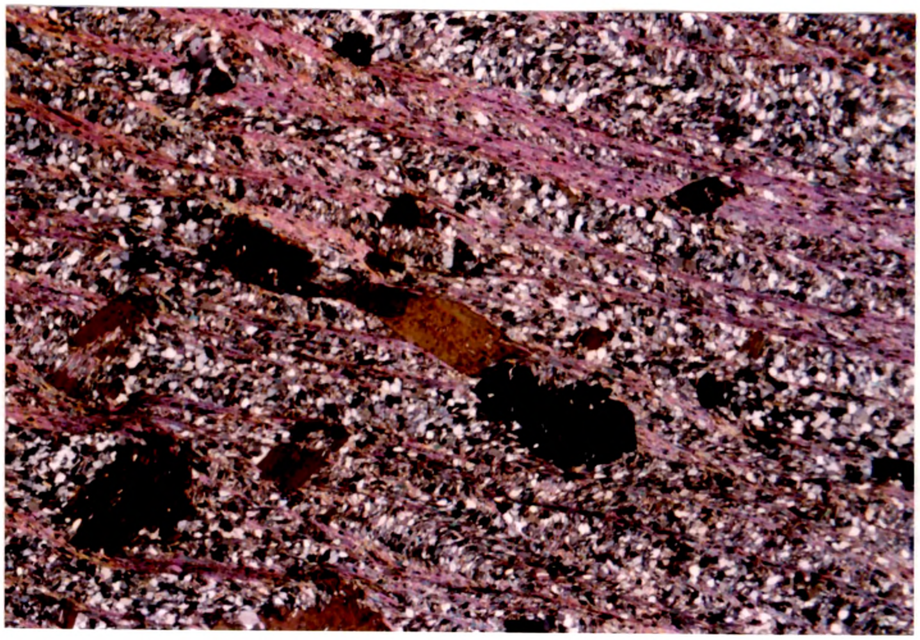

0.4 mm

Fig. 6.7. Photomicrograph of garnet biotite schist. Garnet porphyroblast occurs in contact with biotite porphyroblast. The garnet and biotite porphyroblasts have inclusion trails of quartz which represent S_1 foliation. The crenulation cleavage defined by muscovite rich zones in the matrix marks the S_2 foliation. (X-nicols).

0.1 mm

Fig. 6.8. Photomicrograph of garnet porphyroblast with quartz inclusion trails (S_1). A biotite porphyroblast (top right) coexists with the garnet. The inclusion trails defining the S_1 schistosity within the porphyroblasts are oblique to the external schistosity (S_2) which implies that the garnet and biotite porphyroblasts grew during D_2 deformation. (X-nicols).

possess several porphyroblasts of biotite which preserve microfolded inclusion trails (Fig. 6.9). These are also considered as biotite(2) (pl. see section 6.9 for details). Chlorite occurring along fractures in garnet and biotite and sometimes at the rims of garnet and biotite is designated chlorite(2). The major mineral paragenesis observed are as follows:

a. chlorite(1) + biotite(1) + muscovite + quartz

b. garnet + biotite(1) + muscovite + quartz

c. garnet + biotite(2) + muscovite + quartz

d. garnet + chlorite(1) + biotite(2) + muscovite + quartz

e. biotite(1) + biotite(2) + muscovite + quartz

f. garnet + chlorite(2) + muscovite + quartz

g. biotite(2) + chlorite(2) + muscovite + quartz

Chlorite(1) is observed to occur along the crenulated S_1 schistosity. It has progressed to biotite and garnet during the crenulation event (D_2 deformation). Biotite(2) crystals are generally coarser than biotite(1) suggesting extensive recrystallization during S_2 development. Garnet porphyroblasts have enclosed the microfolded S_1 schistosity as quartz-feldspar inclusion trails (Fig. 6.10 a, b). The study of S_i-S_e relationship has revealed that most of the garnet porphyroblasts develop during the formation of crenulation cleavage (S_2) (see section 6.8 for details). It is obvious that garnet developed progressively from reaction between chlorite and biotite or chlorite, muscovite and quartz (Winkler, 1979).

Large-sized biotite flakes occurring along S_2 foliation (crenulation cleavage) are observed to coexist thus giving the paragenesis - 'e' (above). Rims of some

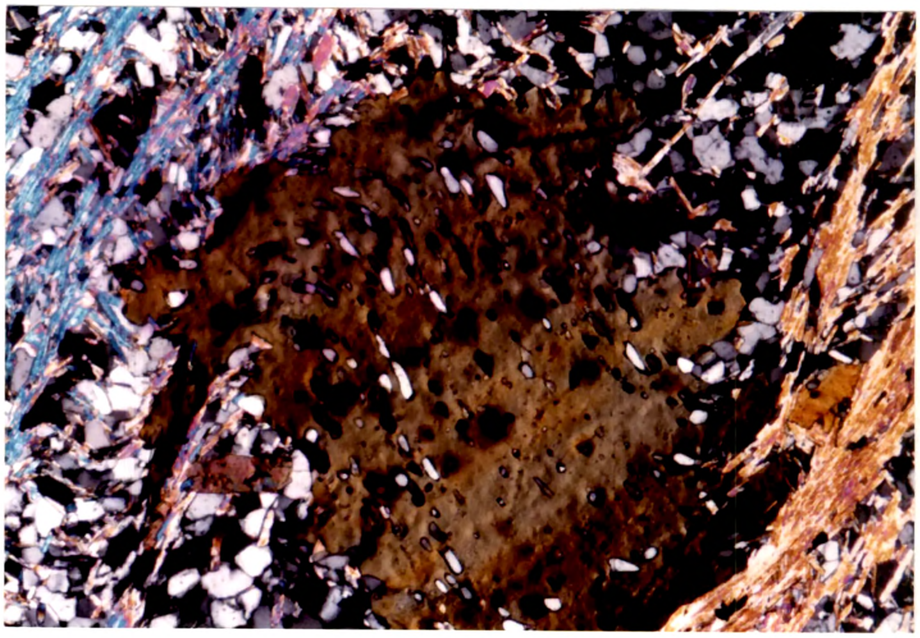

0.2 mm

Fig. 6.9. Photomicrograph of biotite porphyroblast with microfolded quartz inclusion trails. The biotite grew during D_2 deformation. Strong undulose extinction is observed in some of the quartz inclusions which implies a syn-tectonic growth for the biotite. (X-nicols).

a

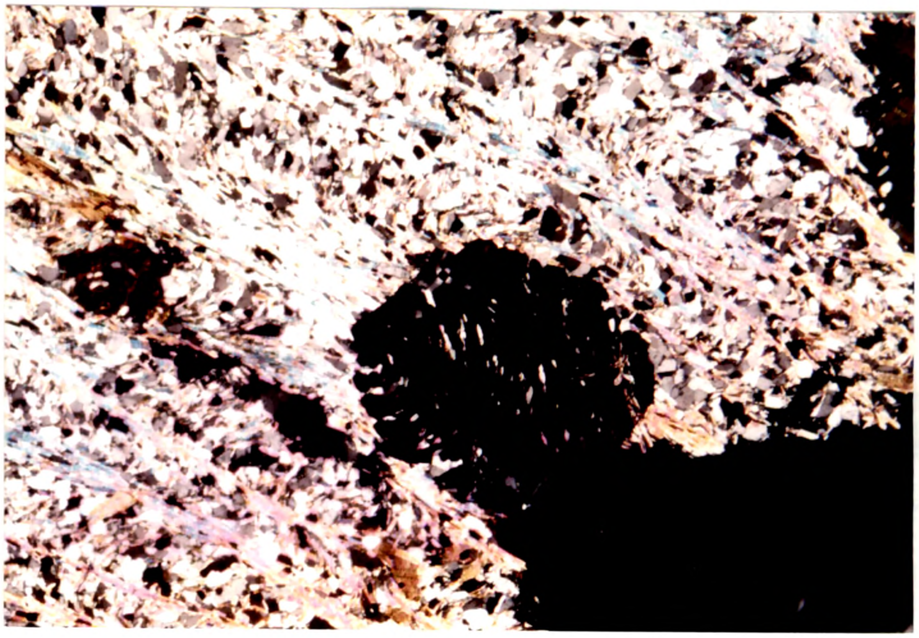

0.4 mm

b

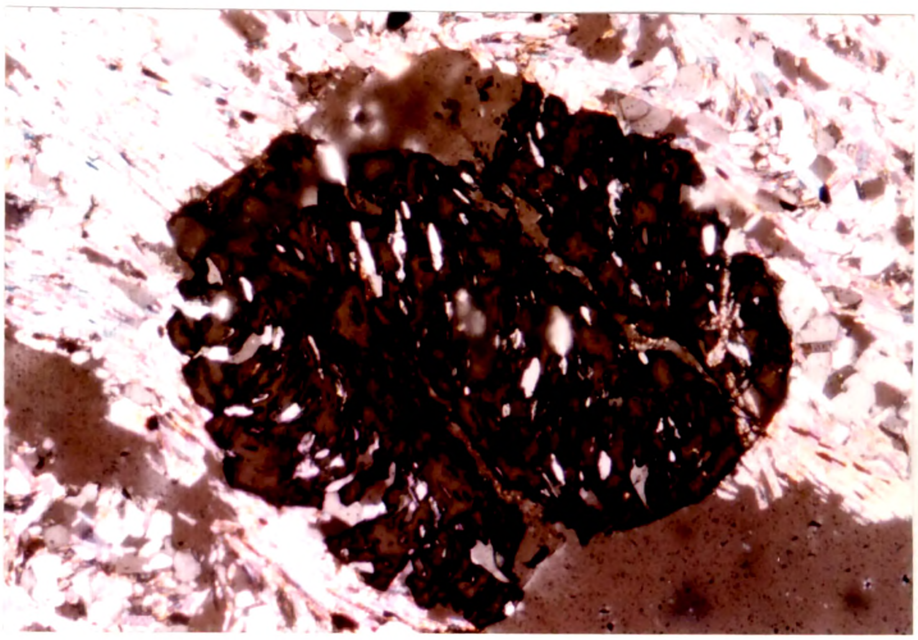

0.1 mm

Fig. 6.10 (a, b). Photomicrographs of garnet porphyroblast which has grown over a crenulation cleavage zone (S_2). The S_1 foliation defined by quartz inclusion trails within the garnet curves sigmoidally into S_2 surface. However, the cleavage zone in the matrix (outside the garnet) is characterized by only a single schistosity (S_2). This implies that the garnet grew over the crenulation cleavage during D_2 deformation. (a, X-nicols; b, partially X-nicols) biotite crystals have changed over to chlorite. This indicates retrogression of biotite and the chlorite is designated as chlorite(2). Another petrographic evidence of retrogression is the presence of chlorite(2) at the rims of porphyroblastic garnet and along fractures in some garnets. The relationship between deformation and related metamorphic events has been dealt with in detail in Section 6.9.

Considering the different mineral assemblages and parageneses present in the garnet-biotite schists, it is obvious that they belong to the lower amphibolite facies. The presence of garnet indicates that the schists fall within the garnet zone. The mineral paragenesis - 'a' (above) indicates that biotite(1) formed by progressive metamorphism of chlorite(1) during the development of S_1 foliation. The mineral paragenesis (b) (above) indicates that the garnet was formed from chlorite(1) and biotite(1) during progressive metamorphism during S_2 formation. The presence of chlorite(2) around garnet and also around biotite(2) indicates retrogressive metamorphism during the waning phases of S_2 development. This is well revealed from the mineral paragenesis - 'f' and 'g' (above).

It is concluded from the above study that the garnet mica schists of the study area first underwent progressive regional metamorphism thus resulting in the formation of garnet. Subsequently the rocks underwent retrogression which was synchronous with the waning phases of D_2 deformation. The third deformation (D_3) which gave rise to open folds in the Lunavada region does not appear to have caused any significant metamorphism. However, the intrusion of the Godhra Granite into the rocks of the Lunavada Group, subsequent to the D_3 deformation, with the accompanying contact metamorphism left its thermal imprints on the rocks. This aspect has been discussed in greater detail in section 6.8.

6.4. CALC-SCHISTS

The calc-schists occur as lensoid bands in association with mica schists and quartzites to the south of Lunavada. These rocks are made up of actinolite, garnet, quartz, sphene, calcite, epidote (zoisite) and chlorite (Fig. 6.11).

There is variation in preferred orientation of different crystals in different parts of the thin section. Some parts show parallelism between actinolite, garnet, quartz and other constituents of the rock. On the other hand in some other parts no preferred orientation is observed and the rock comprises randomly orientated crystals of actinolite, sphene, epidote, chlorite and garnet. Porphyroblasts of actinolite have incorporated quartz grains as inclusion trails (S_i). The S_i in all the randomly oriented actinolite porphyroblasts as well as garnet are parallel to the external foliation (S_e), thereby indicating that the actinolite and garnet have grown in a static condition during the late stage of metamorphism. Actinolite and garnet also show some chloritization. Sphene is xenoblastic. At places garnet appears to have grown in stages as a result of which 'garnet-in-garnet' is present. The inner garnet shows fewer inclusions while the outer one is rich in inclusions where S_i is parallel to S_e. The actinolite-zoisite-garnet-sphene-quartz assemblage also points to epidote-amphibolite facies of metamorphism (Spear, 1993).

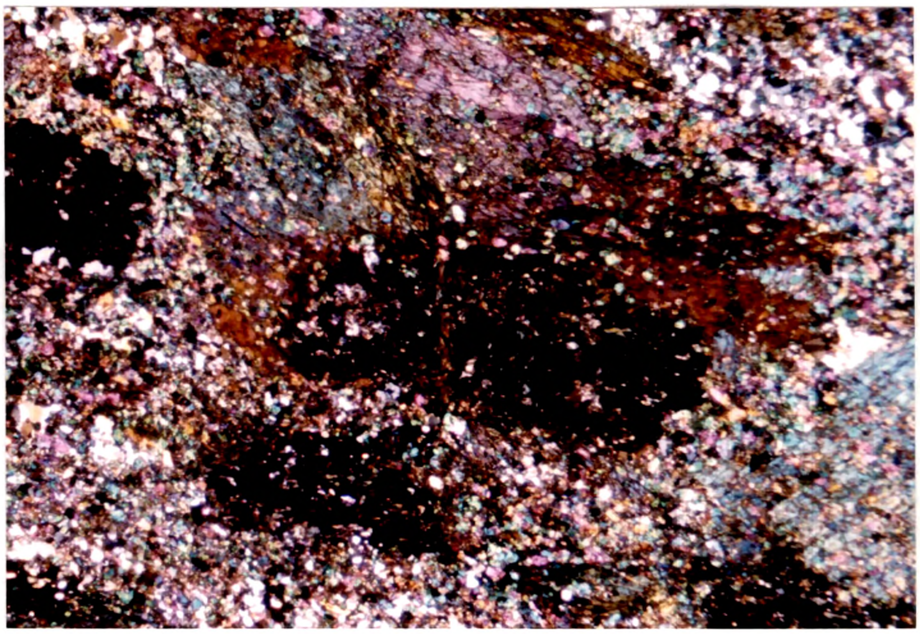

0.2 mm

Fig. 6.11. Photomicrograph of calc-schist. Actinolite, garnet and zoisite are some of the important calcareous minerals which occur in this rock. (X-nicols).

6.5. QUARTZITES

The quartzites of the Lunavada-Santrampur region are generally homogeneous and rarely show any lithological variation. Although a few bands of micaceous quartzites occur at a few places, they generally comprise exclusively of quartz crystals and are usually devoid of any other mineral. However, they do show some interesting microtextures and the study of the type of grain boundaries between quartz crystals throw light on the mechanism and phenomenon of deformation and recrystallization.

Thin sections prepared from different localities of the area show that the quartzites comprise of two textural varieties based on grain boundaries - either the grain boundaries are sutured/serrated or they are straight. The sutured/serrated grain boundaries (Fig. 6.12) are prevalent dominantly in the quartzite occurrences that are distant from the Godhra Granite. According to Urai et. al. (1986) and Passchier and Trouw (1996), the presence of serrated grain boundaries indicates that the rock underwent grain boundary migration recrystallization (GBMR). These show quartz crystals with strong undulose extinction (Fig. 6.13) and this textural feature points to intracrystalline deformation, dynamic recrystallization and the absence of any significant annealing or static recrystallization. On the other hand, thin sections of quartzites occurring closer to the margin of the Godhra Granite show straight grain boundaries, 120° triple points and sharp extinction (Fig. 6.14). The presence of 120° triple points, referred to as foam microstructure by Vernon (1976) is indicative of heat outlasting deformation or annealing. Also, the presence of sharp extinction, straight grain boundaries and coarser grain size of quartz crystals as

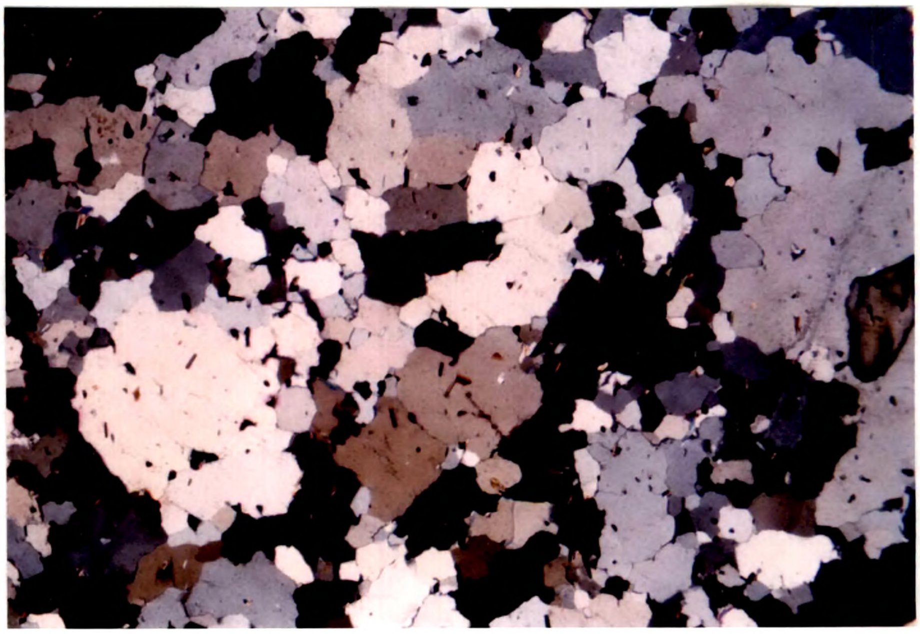

0.2 mm

Fig. 6.12. Photomicrograph of quartz crystals in quartzite showing presence of sutured/serrated grain boundaries implying dynamic recrystallization or GBMR (Grain Boundary Migration Recrystallization) of the rock. (X-nicols).

0.1 mm

Fig. 6.13. Photomicrograph of quartzite showing deformation bands in quartz crystals. The grain boundaries of quartz are serrated. These microstructures imply dynamic recrystallization or Grain Boundary Migration Recrystallization (GBMR). (X-nicols).

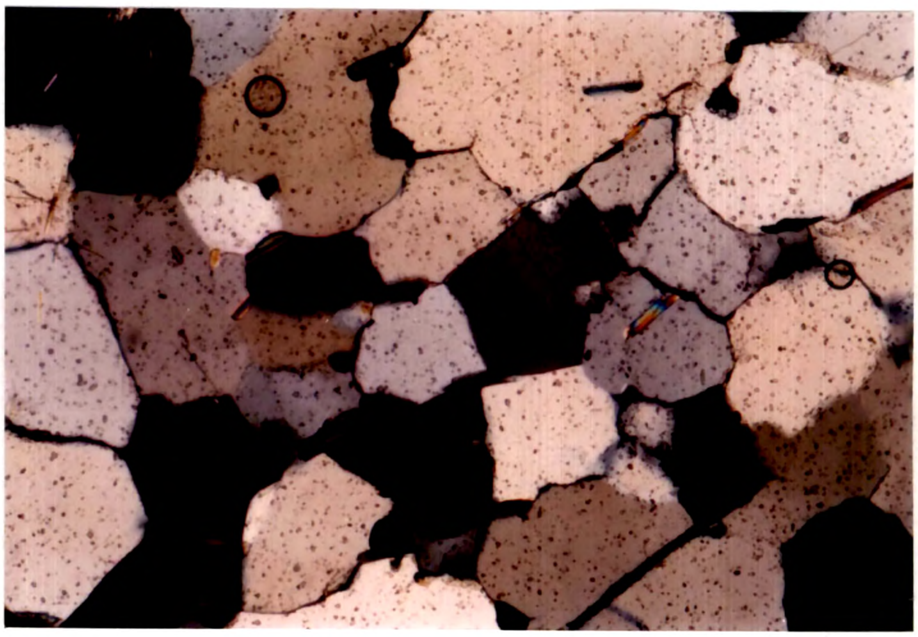

0.2 mm

Fig. 6.14. Photomicrograph of quartz crystals in quartzite showing straight grain boundaries and 120° triple points. The quartz crystals have sharp extinction. These microstructures indicate that the rock underwent static recrystallization. (X-nicols).

compared to those lying farther from the granite , indicates that the quartzites closer to the granite underwent static recrystallization by *Grain Boundary Area Reduction* (GBAR) or annealing (Passchier and Trouw, 1996). Obviously, the heat energy required for the above came from the Godhra Granite which has intruded the Lunavada Group metasediments. This microstructural study further supports the conclusions made by the author using Crystal Size Distribution (CSD) data (section 6.8).

It has been logically postulated that prior to metamorphism the quartz crystals were in a high strain condition and characterized by undulose extinction and they must have undergone dynamic recrystallization syntectonically resulting into the development of serrated grain boundaries. As the rocks of the study area have undergone metamorphism only upto lower amphibolite facies, it is obvious that the deformation took place at relatively low temperatures. According to a number of workers (Hobbs et. al., 1976; Spry, 1969; Vernon, 1976 and Nicolas and Poirier, 1976) deformation of a crystal at relatively low temperatures and /or high strain rates results in the increase in dislocation density and formation of dislocation tangles or pile-ups. This phenomenon is similar to cold-working in metals. The increased dislocation density causes the crystal to harden and thus more stress is required to further deform the crystal. This phenomenon has been referred to as work-hardening (Ghosh, 1985). A cold worked crystal is characterized by a higher internal energy than the undeformed crystal and is thermodynamically less stable. It is hypothesized that such must have been the state of the quartz crystals in the quartzites under investigation during the deformation and they must have been in a cold worked state. Subsequent to the deformation, the rocks were intruded by the Godhra Granite which caused a rise in temperature of the surrounding rocks. With increasing temperature, the cold worked state tends to become increasingly unstable and eventually the crystal softens and reverts to a strain-free condition, a phenomenon termed as annealing (Ghosh, 1985; Dieter, 1988). This process involves recovery, recrystallization and grain growth and results in reduction of dislocation density, coarsening of the grain size with concomitant reduction in the total number of grains to achieve greater thermodynamic stability. As a result, the initial cold worked state of the quartz crystals in quartzites changed to a more stable state by the process of annealing due to the heat supplied by the Godhra Granite, thus resulting in the straightening of grain boundaries and development of 120° triple points. This effect was significant in the quartzites lying closer to the margin of the Godhra Granite, lying to the south of Lunavada but was insignificant in the quartzites which lie at a greater distance from the granite. As a result the latter show serrated/sutured grain boundaries, stronger undulose extinction, finer crystal size and larger number of crystals in unit area all of which suggest that the rock could not release its internal strain due to its greater distance from the heat source.

6.6. DIFFERENTIATED CRENULATION CLEAVAGE

Garnet biotite schists of the study area around Lunavada have preserved some interesting microstructures which deserve an exclusive description and detailed discussion. Of these, the most prominent microstructure is the differentiated crenulation cleavage (S_2) which is defined by alternating quartz-rich(Q) and mica-rich (M) domains. The crenulation cleavage is the schistosity S_2 which formed due to the microfolding of the pre-existing foliation S_1 during D_2 deformation. A careful observation of the cleavage zones (M domains = S_2) has revealed the presence of following microstructures that resemble those found on the mesoscopic scale in *Ductile Shear Zones (DSZs)*;

(a) In several M-domains the S_1 surfaces defined by mica aggregates, progressively curve sigmoidal and become parallel to the domain boundary (S_2 surface) (Fig. 6.15).

(b) In some M-domains, a cleavage S_2' is observed to be present. The important characteristics of S_2' are; (i) S_2' forms at a low angle (less than 45°)to the foliation S_2 (domain boundary); (ii) in the domains where it is well developed it imparts a 'button schist' appearance to the M-domains; (iii) there is no evidence of metamorphic differentiation during the formation of S_2'. This suggests that S_2' defines a real plane of displacement rather than volume loss. Fig. 6.16 shows S_2' in its embryonic stage of development while in Fig. 6.17 a well developed S_2' giving a button schist appearance to the M-domain is seen.

There is a striking resemblance between the microstructures described in (a) and (b) above and those described from DSZs. Fig. 6.15b shows the progressive sigmoidal curving of S_1 into S_2 which resembles the *S-C (Schistosité-Cissilament)* fabric commonly known to occur in mylonites from DSZs (Berthé et al. 1979; Lister and Snoke, 1984; Ghosh, 1985). Similarly the microstructural characteristics related to S_2' surface in Fig. 6.17resemble the *Extensional Crenulation Cleavage (ECC)* that have been described from DSZs (Berthé et al., 1979; Platt and Vissers, 1980; Blenkinsop and Trealor, 1995). It is important to mention that although the mica schists presently under scrutiny do not belong to a mylonite zone, the differentiated crenulation cleavages have preserved within them microstructures resembling S-C

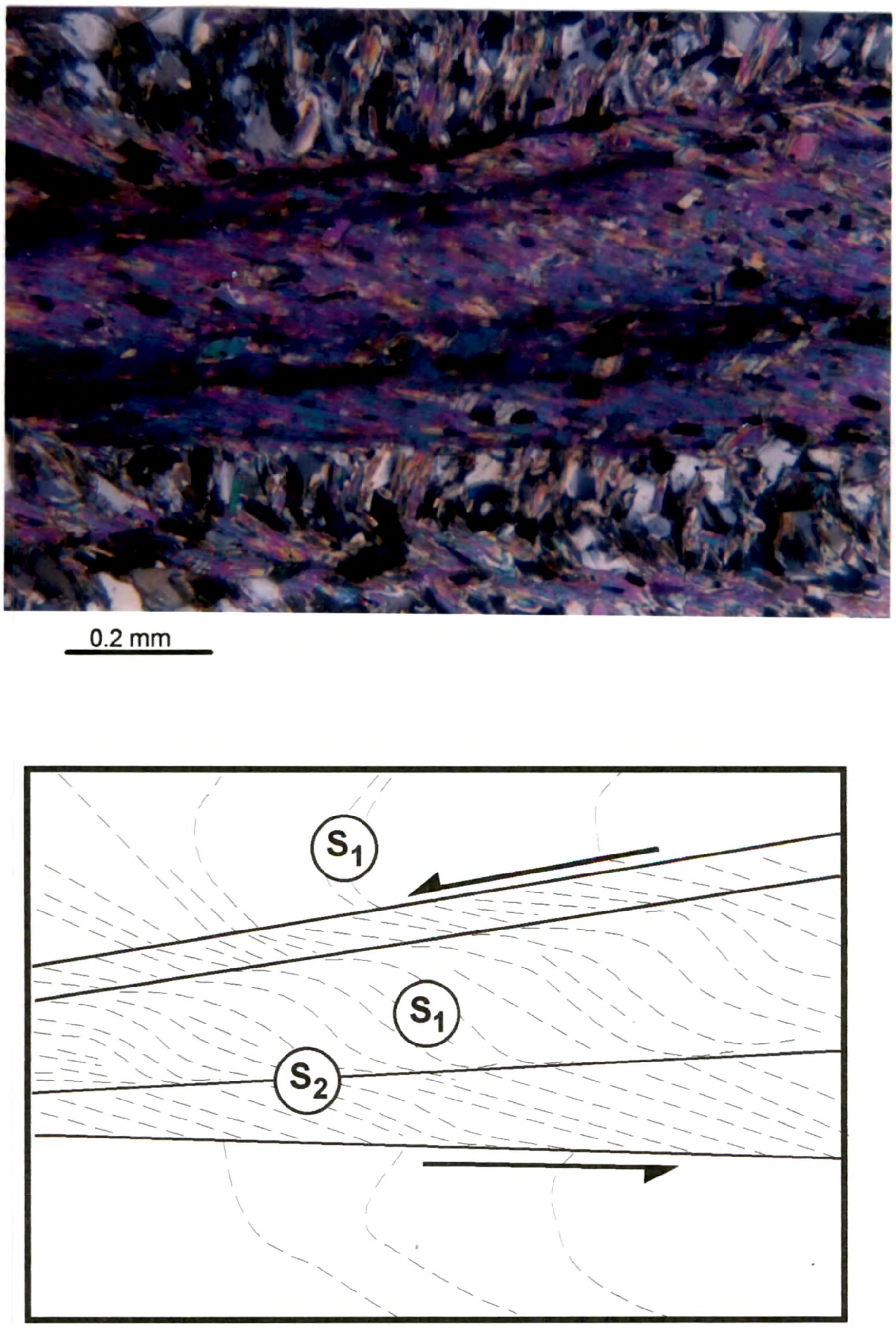

Fig. 6.15. (a)Photomicrograph of cleavage zone (Mica-domain/M-domain) in mica schist. The mica aggregates defining the S_1 foliation within the M-domain curve sigmoidally into the S_2 surface (domain boundary). The fabric is similar to the S-C fabric which normally occurs in Ductile Shear Zones. (X-nicols).
(b) Explanatory line drawing of microstructural relationships observed in (a).

a

b

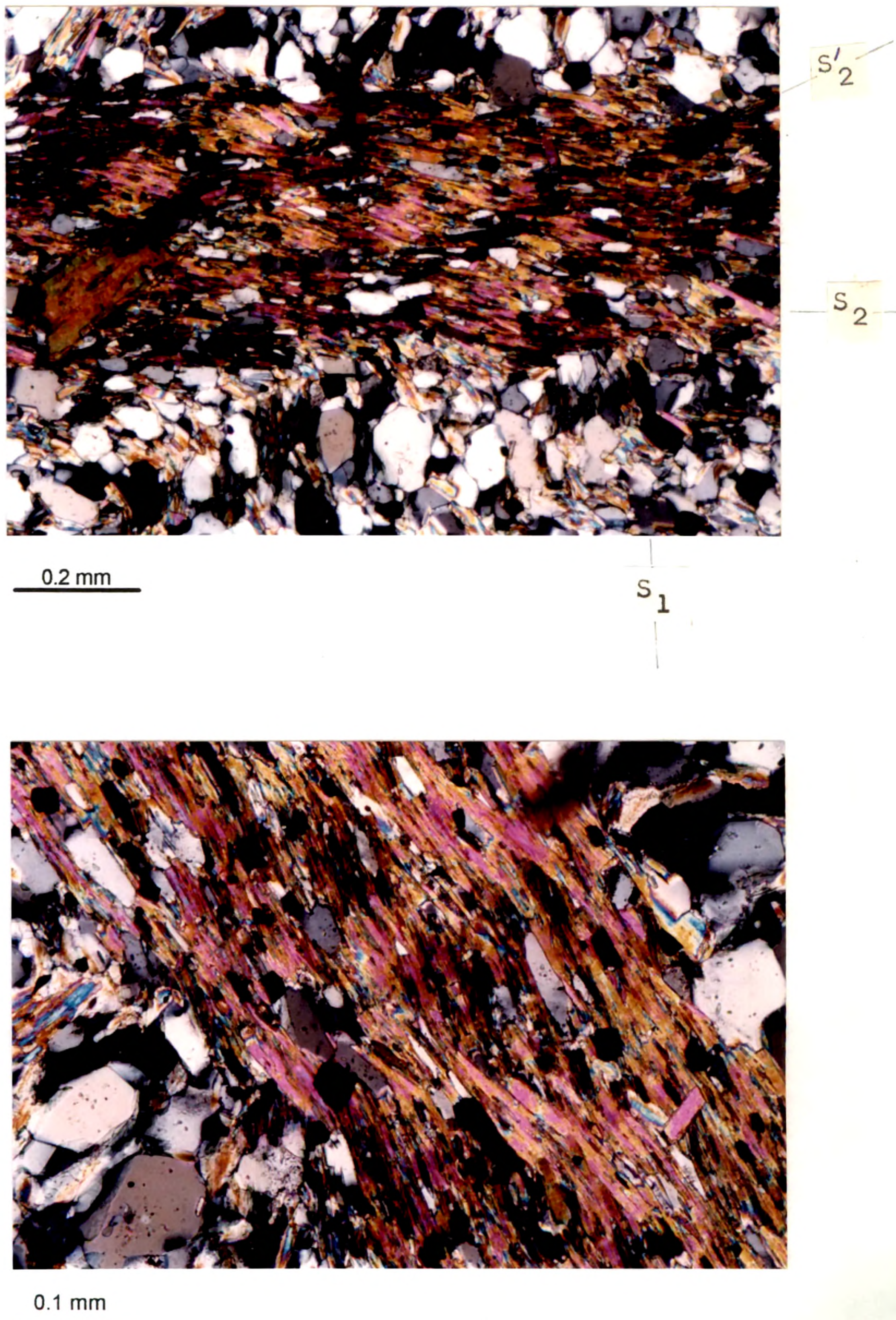

Fig. 6.16 (a, b). Photomicrograph of cleavage zone (M-domain) in mica schist showing presence of an embryonic S_2' surface at a low angle to S_2 (domain boundary). (X-nicols).

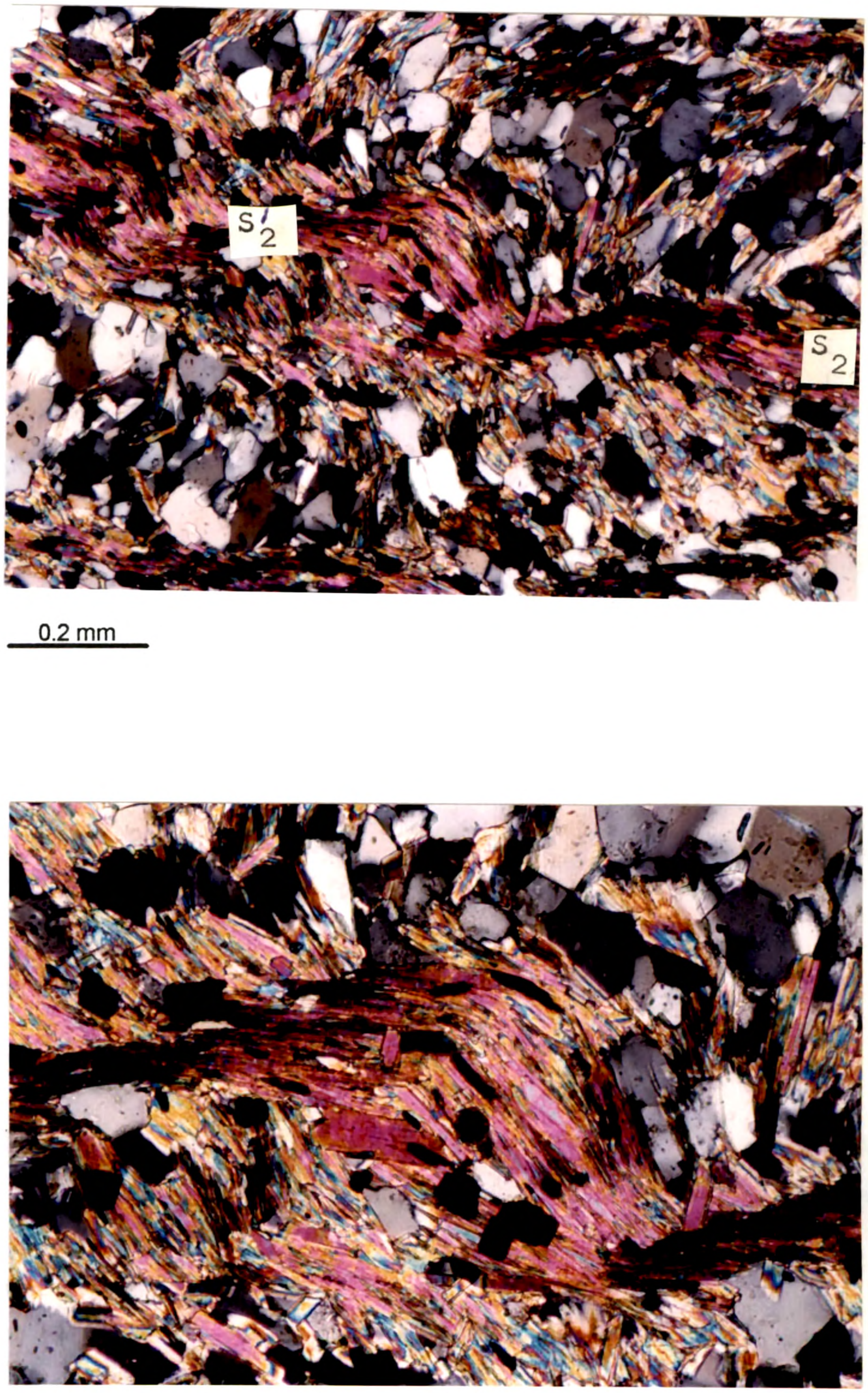

a

0.2 mm

b

0.1 mm

Fig. 6.17 (a, b). Photomicrograph of cleavage zone (M-domain) in mica schist showing development of a well developed S_2' at low angle to the domain boundary (S_2). The S_2' resembles C' fabric (shear bands) which commonly occur in Ductile Shear Zones. X-nicols.

and ECC fabrics which have so far been known to develop in mylonites from DSZs. It can be therefore stated that crenulation cleavages in the mica schists of the study area behaved as microscale shear zones during D_2 deformation. During shearing along the cleavage zones, the S_1, S_2 and S_2' surfaces perhaps behaved as S, C and ECC (or C') surfaces respectively. On the basis of these microstructures, a sequence of events is invoked for the genesis of crenulation cleavages in rocks.

Microfolding of the pre-existing foliation S_1 resulted in the initiation of the differentiated crenulation cleavage (S_2). During the initial stages of microfolding (crenulation), solution transfer resulted in the migration of quartz from the limbs of the microfolds to the hinges, whereas the phyllosilicates got concentrated in the limb regions. This led to the formation of the domainal fabric in the rock which is characterized by alternating Q and M domains (Williams, 1972, 1978; Means and Williams, 1972; Cosgrove, 1976; Marlow and Etheridge, 1977; Gray, 1977, 1978, 1979). Volume was lost during this process at least on the scale of a few microfolds, although this is not essential on a larger scale (Mancktelow, 1994). After the rock achieved its domainal fabric, the M-domains define a zone of strong anisotropy characterized by S_1 mica aggregates. Shearing occurred along the M domains and this resulted in the progressive sigmoidal curving of S_1 foliation within the M domains into parallelism with the domain boundary (S_2 surface) (Fig. 6.15). The microstructures thus formed resemble the S-C fabric of DSZs. Continued shearing along these domains resulted in the formation of S_2' surface at a low angle (less than 45°) to the domain boundary (S_2 surface) within the M domain of the differentiated crenulation cleavage (Fig. 6.17). The S_2-S_2' relationship is similar to the ECC of DSZs (see Blenkinsop and Trealor, 1995 for e.g.). Volume was conserved during the development of S_2' because metamorphic differentiation on account of solution transfer had already occurred to a large extent durıng the earlier stages of the formation of crenulation cleavage (S_2).

Bell and Rubenach (1983) proposed a six-stage model for origin of crenulation cleavages in rocks. Their model does not include the development of microstructures resembling S-C and ECC in M domains. Mamtani and Karanth (1996a) proposed a new model for the formation of crenulation cleavages in rocks to incorporate the microstructures developed along M-domains of the differentiated crenulation cleavages. Fig. 6.18 shows their model simulating development of crenulation cleavage (S_2) from a pre-existing foliation S_1. Accordingly, the rock achieves its domainal fabric by stage 3. Solution transfer or pressure solution is the dominant process upto stage 3 during which quartz migrates from the limbs to the hinges of the microfolds. Shearing along M domains becomes significant from stage 4a and results in the development of a structure similar to S-C fabric found in mylonites. Continued shearing along the M domains results in the initiation of an embryonic S_2' surface in stage 4b and finally a well developed S_2' surface develops in stage 4c, which is similar to ECC found in mylonites. With further deformation S_2' surfaces in M domains totally rotate into parallelism with the domain boundary and the relict crenulations in Q domains are destroyed. This is stage 5 of crenulation cleavage genesis. Finally, in stage 6 the foliation gets homogenized.

According to Gray (1979) all crenulation cleavages are pressure solution surfaces and no appreciable movement occurs "at any stage" of their development. Interestingly, the microstructural investigation of the mica schists carried out by the

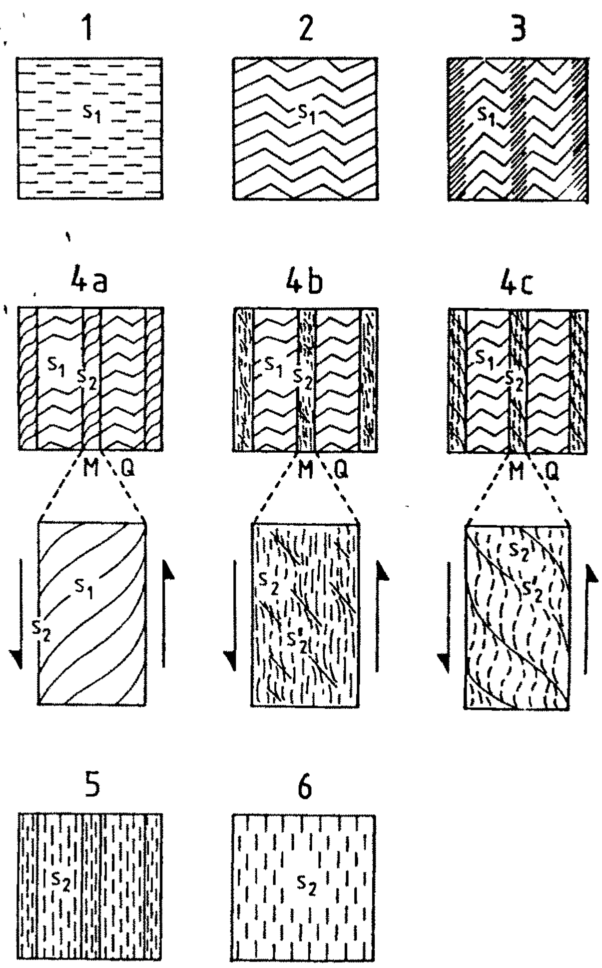

! How do you attribute between 1 and 6

Fig. 6.18. Model showing the sequential development of microstructures in M-domains during crenulation cleavage development. Solution transfer and resultant metamorphic differentiation dominate upto stage-3. From stage-4a, the domain boundary starts behaving as a shear surface and results in the development of fabric resembling S-C fabric which occurs in rocks from Ductile Shear Zones. With increasing strain and shearing along M-domains, an embryonic S_2' surface initially develops at a low angle to S_2 in stage-4b and subsequently a well developed S_2' is formed in stage-4c. S_2' resembles ECC (shear bands) found in Ductile Shear Zones. In stage-5 the relict crenulations in Q-domains are destroyed and S_2' surfaces in M-domains rotate into parallelism with domain boundary. In stage-6, the S_2 foliation gets homogenized. Compare stages 4a, 4b and 4c with figures 6.15, 6.16 and 6.17 respectively. (Fig. is after Mamtani and Karanth, 1996a).

present author has revealed that a crenulation cleavage can behave as both, a pressure solution surface and as a ductile shear zone during different stages of its development. Pressure solution (solution transfer) is undoubtedly the dominant mechanism during the earlier stages of crenulation (upto stage 3 in Fig. 6.18) and due to this phenomenon the rock achieves its domainal fabric. However, the presence of microstructures resembling S-C and ECC fabrics within the cleavage zones (M domains) suggests that the crenulation cleavages behave as microscale shear zones during the later stages of crenulation (i.e. stage 4a onwards). This is in conformity with the suggestion made by Williams and Schoneveld (1981) that the S_2 surface becomes an active surface of shear after all the mobile material has been removed from it. It is important to note here that volume is lost from the cleavage zones upto stage 3 of crenulation cleavage development. Subsequently, intracrystalline deformation occurs along the M domains due to shearing. That intracrystalline deformation does occur is ideally revealed by the undulose extinction of some mica aggregates along the embryonic S_2' surfaces in Figs. 6.16 and 6.17. However, the presence of recrystallized fine mica aggregates along well developed S_2' in Fig. 6.17 suggests that recrystallization also occurs during later stages of crenulation. The present study thus reveals that crenulation cleavages in schists of the study area were initiated due to pressure solution related to microfolding during D_2 deformation and later on underwent intracrystalline deformation and syntectonic recrystallization during the later stages of the same D_2 deformation.

6.7. MILLIPEDE MICROSTRUCTURE

Another interesting microstructure preserved in the garnet-biotite schists is the *millipede microstructure*. The millipede microstructure characterized by *Oppositely Concave Microfolds* (OCMs) were first reported in naturally deformed schists by Bell and Rubenach (1980). The millipedes are usually preserved in the form of OCMs of quartz inclusions within porphyroblasts in schists. Bell and Rubenach (1981) stated that the presence of millipede microstructure indicates that the rock underwent coaxial deformation. Millipedes have been interpreted similarly by Bell (1985), Bell et al. (1986, 1992), Bell and Cuff (1989), Bell and Hayward (1989), Bell and Johnson (1989), Hayward (1990), Johnson (1990a, b; 1992; 1993a, b), Gururajan (1994), Aerden (1995). However, Passchier et. al. (1992) have disagreed with this interpretation by stating that similar microstructures could also develop during bulk simple shear. Several workers have shown that structures similar to millipede microstructure can develop around rotating rigid objects at low strains in laboratory experiments done in simple shear as well as general type of deformation (i.e. with both pure and simple shear components (Ghosh 1975, 1977; Ghosh and Ramberg, 1976). Johnson and Moore (1996) and Johnson and Bell (1996) have reviewed the applicability of millipedes in determining deformation histories of rocks and have concluded that the millipedes indicate the low strain state only and should not be used to interpret bulk deformation histories.

Millipede microstructures characterized by OCMs comprising quartz inclusion trails are observed in porphyroblasts of biotite in the mica schists of the Lunavada region (Figs. 6.19 a, b and 6.20 a, b). The porphyroblast growth is syntectonic with D_2 deformation as is interpreted by the porphyroblast - matrix relationship and also

a

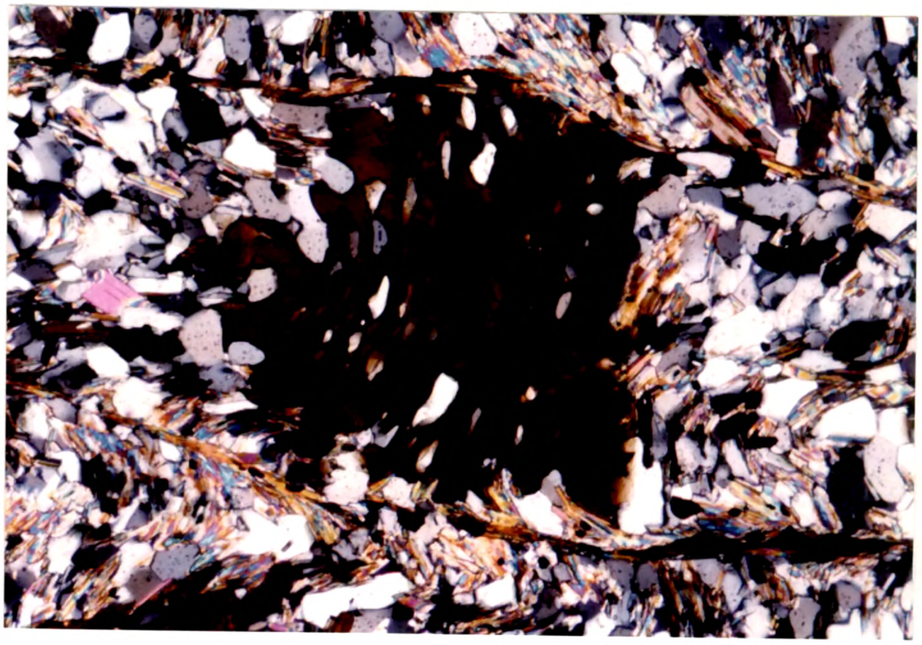

0.1 mm

b

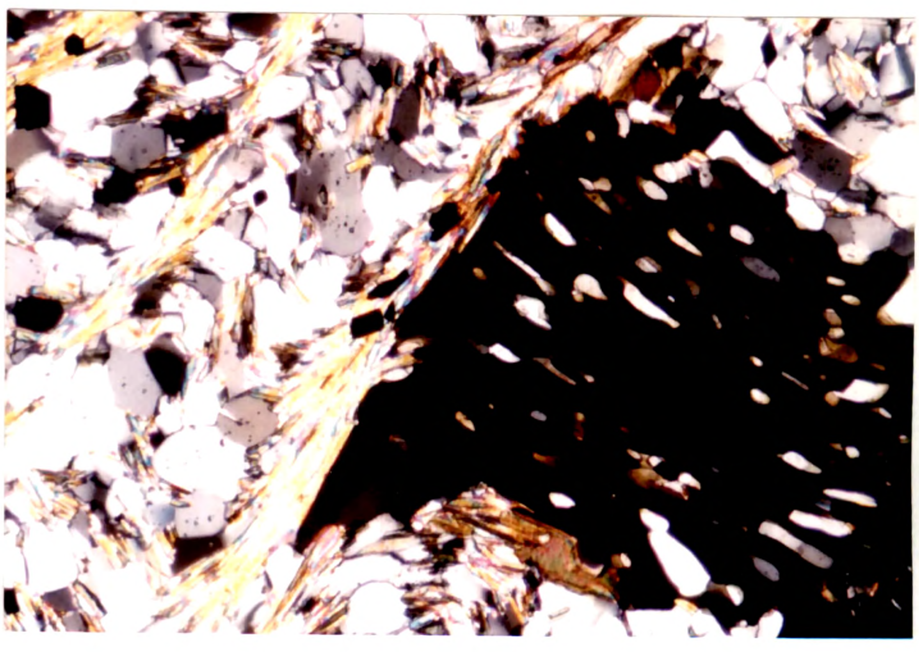

0.1 mm

Fig. 6.19 (a, b). Photomicrographs of biotite porphyroblasts in garnet-biotite schist showing presence of millipede microstructure. The millipedes are characterized by oppositely concave microfolds (OCMs) of quartz-feldspar inclusion trails (S_1) within the porphyroblasts. (X-nicols).

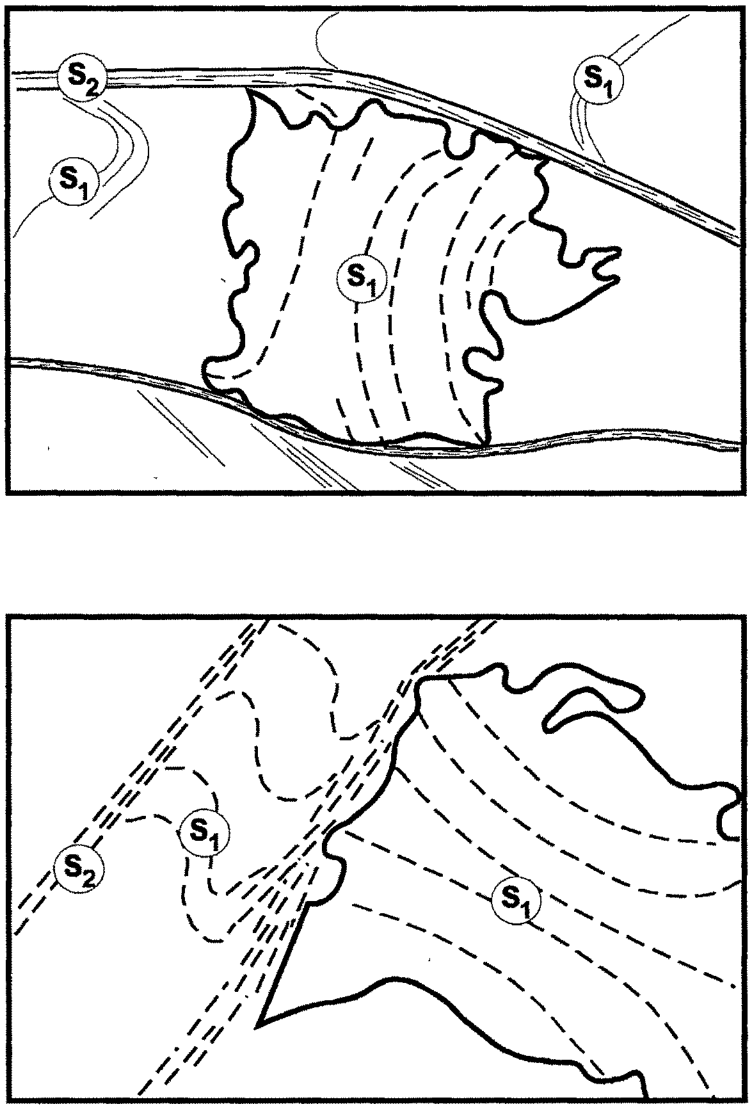

a

b

Fig. 6.20 (a, b). Explanatory line drawings of the millipede bearing biotite porphyroblasts in fig. 6.19a and b respectively.

the undulose extinction of some quartz inclusions. It is observed that the S_1 foliation outside the porphyroblast is tightly crenulated as compared to the S_1 foliation within the porphyroblasts which is only slightly curved. This indicated the millipede bearing porphyroblasts grew during early stages of D_2 deformation when the strain was relatively low. This is in conformity with the suggestion of Johnson and Bell (1996) and Johnson and Moore (1996) that the presence of millipedes indicates the low strain state at the time of porphyroblast growth. This would also support the observation of structures similar to millipedes observed to develop at low strains in the laboratory experiments done by Ghosh (1975, 1977), Ghosh and Ramberg (1976) and Masuda and Ando (1988). However, the present author would like to state that symmetrical microfolds are observed in the Q-domains adjacent to the millipede bearing porphyroblasts. Also, the S_1 quartz inclusion trails marking the millipedes are near perpendicular to the S_2 foliation outside the porphyroblast. These microstructural relationships seem to suggest that perhaps the microarea preserving the millipede-bearing porphyroblast might have undergone coaxial deformation.

rods are due to grain growth ?.

6.8. CONTACT METAMORPHISM AND RELATED "CSD" STUDIES ON QUARTZ

The regional metamorphism in the Lunavada-Santrampur region was followed by an event of thermal metamorphism related to the contact effect of Godhra granite. The effects of heat supplied by the Godhra granite are significant in the southwestern part of the study area i.e. to the south of Lunavada. Since the granite does not lie in the immediate vicinity of the study area, contact metamorphic minerals like andalusite and sillimanite are absent in the rocks. Nevertheless the effect of the thermal event is quite obvious from the *Crystal Size Distribution* (CSD) studies on quartz crystals in schists and quartzites.

6.8.1. CSD studies on quartz

The CSD theory was first formulated and adapted in chemical engineering literature by Randolph and Larson in 1971 and subsequently applied to earth sciences (Marsh, 1988). It has been used to understand the effect of heat on crystal sizes in rocks, to calculate nucleation and growth rates of crystals, the growth time of crystals in igneous and metamorphic rocks (Marsh, 1988; Cashman and Ferry, 1988; Cashman and Marsh, 1988). The fundamental steps involved in CSD measurements are described below.

An area of 1 cm^2 thin section is selected. Measurement of longest crystal dimension of all the grains of a particular mineral being studied (in this case quartz) are made for the selected area. This gives the frequency distribution of crystals (N_A) of various sizes (L) in the unit area. Using the formula $N_V = N_A^{1.5}$, the number of crystals of size L in unit volume (N_V) is determined. N_V is the true grain size distribution. From these data the volume frequency histogram (N_V vs. L) is prepared, which provides a good graphical representation of the distribution of crystals of different sizes. Subsequently, the population density (n) of the crystals of different size is calculated. Population density (n) is defined as the number of crystals in a given size class per unit volume and is obtained by the formula

$$n = N/L = dN/dL$$

where N is the cummulative number of crystals per unit volume. The plot of $l_n(n)$ against L is referred to as the CSD plot and the shape of this plot is the

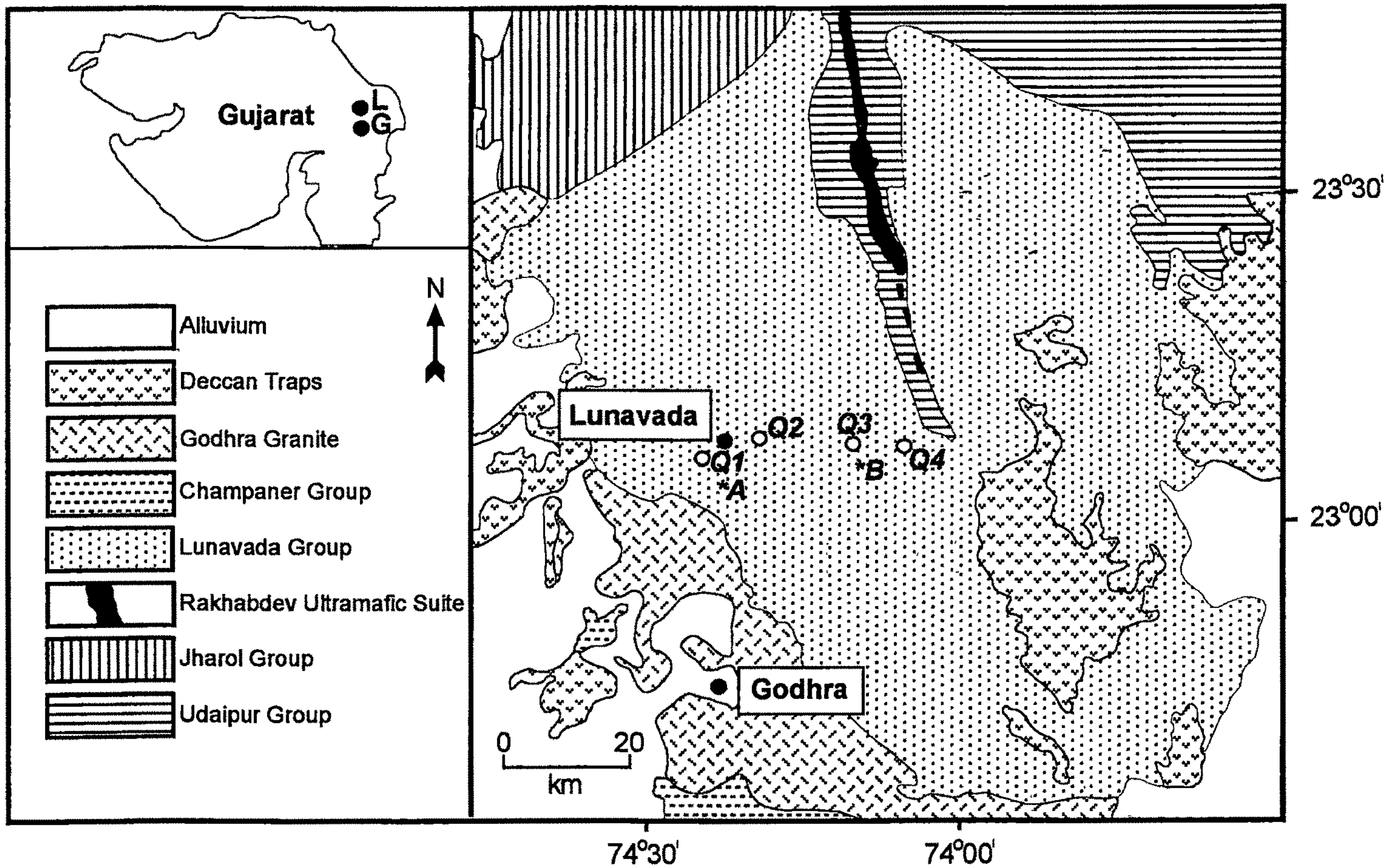

Fig. 6.21. Map showing the locations from which samples of schists and quartzites were collected for CSD study. Inset: L is Lunavada, G is Godhra. Schist samples A and B are represented by star. Q1, Q2, Q3 and Q4 represented by open circles are quartzite samples.

manifestation of the effect of heat on the CSDs and gives a convincing graphical representation of the extent of annealing the rock underwent.

Using the above principles and steps, CSDs of quartz grains were calculated in thin sections of two schist samples and four quartzite samples, all collected systematically at varying distances from the boundary of the Godhra Granite. Fig. 6.21 shows the location of the samples of schists and quartz samples.

(a) CSD study of quartz in schists

Thin sections of two schist samples collected at 4 km (Sample A) and 22 km (Sample B) from the margin of the Godhra Granite were subjected to CSD analysis and the total number of quartz crystals in unit area (N_A) in the two samples were found to be 1225 and 5931 respectively. Using the CSD theory described above, the number of crystals in unit volume were calculated for each size class from which the population density (n) was obtained. Table 6.2 a, b show the data obtained for each of the two samples respectively. Figures 6.22 a, b are the volume frequency histograms (N_V vs. L) for the respective two samples. Fig. 6.22a is the volume frequency histogram for the sample close to the granite. It shows that the quartz crystals have crystallized over a wide range with the maximum frequency being in the intermediate size range. On the other hand, the quartz grains in the sample away from the granite have crystallized in a limited size range and the maximum frequency is in the smaller size range (Fig. 6.22b). Fig. 6.23 is the CSD plot for the samples close and far from the margin of the Godhra Granite respectively. It is observed that the CSD plot for the sample close to granite is distinctly different from the CSD plot of sample far from the granite margin. The former shows a bell shaped CSD plot while the latter is more or less linear. These different shapes of the CSD plots reflect the varied thermal histories of the respective samples. Linear CSDs have been described for crystals in igneous rocks and hornfelses and have been interpreted to indicate continuous nucleation and growth of crystals (Cashman and Ferry, 1988; Cashman and Marsh, 1988)

This is probably a [illegible] [illegible] [illegible] be [illegible]

Table 6.2a

CSD Data for schist lying close to the Godhra Granite (Sample A)

L (mm)	N_A (no./cm^2)	N_V (no./cm^3)	n (no./cm^4)	ln(n)
0.025	013	0046.87	00937.44	06.84
0.075	245	3834.85	76697.13	11.24
0.125	217	3196.60	63932.19	11.06
0.175	260	4192.37	83847.48	11.33
0.225	242	3764.63	75292.73	11.22
0.275	105	1075.92	21518.59	09.97
0.325	067	0548.41	10968.37	09.30
0.375	038	0234.24	04684.95	08.45
0.425	019	0082.81	01656.38	07.41
0.475	007	0018.52	000370.4	05.91
0.525	006	0014.69	00293.93	05.68
0.575	002	0002.82	00056.56	04.03
0.625	003	0005.19	00103.92	04.64
0.675	001	0001.00	00020.00	02.99

Table6.2b

CSD data for schist lying far from the Godhra Granite (Sample B)

L (mm)	N_A (no./cm^2)	N_V (no./cm^3)	n (no./cm^4)	ln(n)
0.025	3200	181019.33	3620386.71	15.10
0.075	2515	126126.68	2522533.71	14.74
0.125	0195	002723.02	0054460.53	10.90
0.175	0021	000096.23	0001924.68	07.56

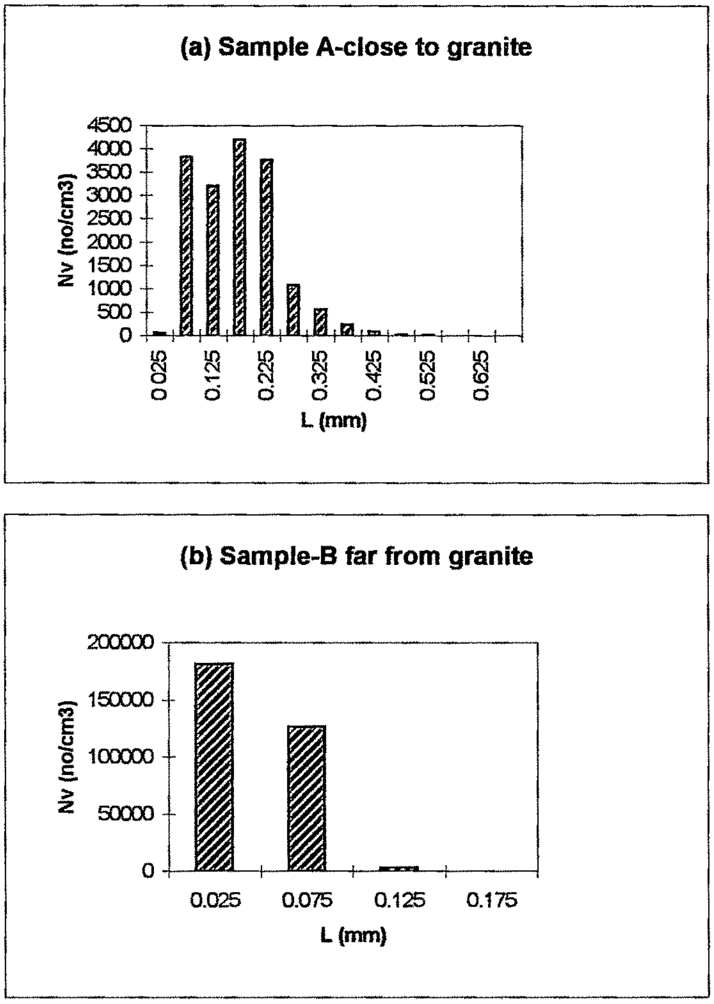

Fig. 6.22. Volume frequency histograms (Nv vs L)for quartz crystals in schist

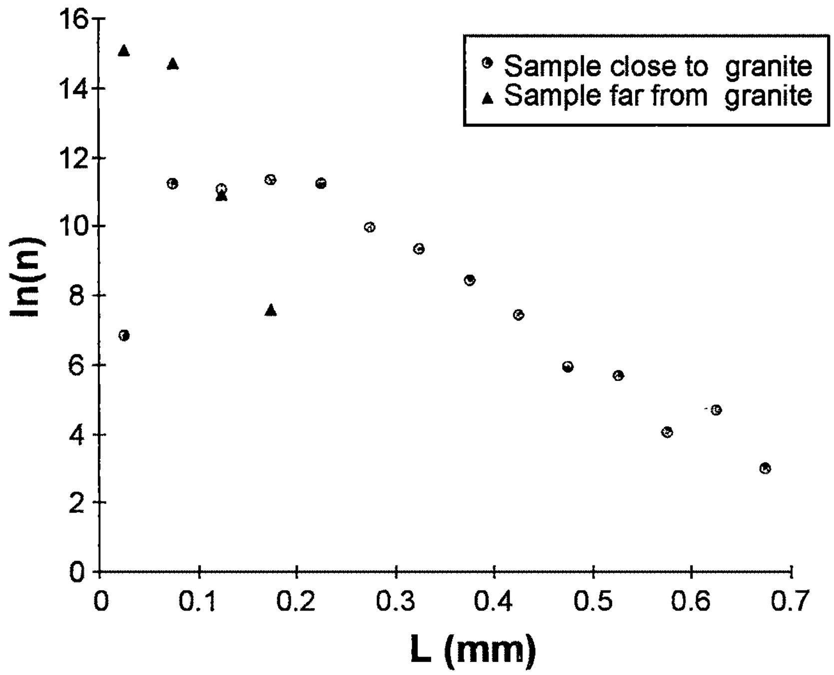

Fig. 6.23. CSD plot for schist samples

On the other hand, bell shaped CSDs have been described for minerals like garnet and sphene in regionally metamorphosed rocks and are considered to indicate (i) an initial continuous nucleation and growth of crystals, and (ii) later loss of small crystals due to annealing (Cashman and Ferry, 1988; Cashman and Marsh, 1988). Accordingly, it is interpreted that the bell shaped CSD plot obtained for the sample closer to the granite in Fig. 6.23 indicates strong annealing. The initial growth of quartz crystals in the above two rocks was continuous which is indicated by the linearity of the right hand portion of the bell-shaped CSD plot which represents ln (n) at larger values of L. Subsequently, the smaller crystals were resorbed at the expense of the larger crystals due to annealing which was triggered by the heat supplied by the intrusion of the Godhra granite and resulted in prolonged cooling at high temperatures. It is this later phenomenon which gives the bell shape to the CSD plots. Contrary to these samples, the sample of schist which is 22 km away from the margin of the Godhra granite does not show any significant bell shape and has a higher slope which suggests continuous nucleation and growth.

Table 6.3 clearly indicates that the sample closer to granite has lesser number of quartz crystals in unit area, a larger mean crystal size and crystallized over a wider size range all of which are due to annealing related enhanced growth of the quartz crystals on account of heat supplied by the Godhra Granite (Mamtani and Karanth, 1996b).

Table 6.3
Comparative results from CSD study of schists

Sample No.	N_A	Mean Size (mm)	Size Range
A	1225	0.1851	0.025 - 0.675
B	5931	0.05	0.025 - 0.175

(b) CSD study of quartz in Quartzites

The study of CSDs of quartz similar to that described above was also carried out on the quartzites of the Lunavada Group using *Omnimet Analyzer* with the assistance of Professor Bruce March and Micheal Zeig of John Hopkins University, USA. Four thin sections of quartzites (numbered Q1, Q2, Q3 and Q4 respectively) lying at a distance of 4, 10, 22 and 30 km from the margin of the Godhra Granite were studied and the respective CSD data of ln(n) vs. L is given in the tables 6.4 a,b.

The CSD plots for the four quartzites are plotted in Fig. 6.24 respectively. These plots show that the slope of the CSD plots decreases as the granite is approached, thus suggesting that the quartzites closer to the granite underwent extensive annealing. This confirms the interpretations of Mamtani and Karanth (1996 b) on the basis of CSD data of quartz crystals in schists of the Lunavada Group.

Is it really necessary to do such an exercise to say that uniform grain indicates recrystallization at the border!

Table 6.4 a

CSD Data for Quartzites in Lunavada region (Samples Q1 and Q2)

Size L (mm)	ln(n) Sample Q1	ln(n) Sample Q2
0.00	00.00	00.00
0.05	11.18	11.58
0.10	11.32	11.80
0.15	10.82	11.52
0.20	10.13	11.10
0.25	09.48	10.60
0.30	08.92	10.28
0.35	08.52	09.96
0.40	08.56	09.39
0.45	07.94	08.69
0.50	06.75	08.39
0.55	07.56	08.14
0.60	07.62	07.64
0.65	07.63	07.40
0.70	06.77	07.62
0.75	05.27	07.38
0.80	05.98	06.58
0.85	05.91	05.92
0.90	06.91	04.72
0.95	06.45	04.60
1.00	05.43	05.21
1.05	04.91	04.43
1.10	05.56	00.00
1.15	04.82	00.00
1.20	00.00	04.61
1.25	04.72	04.61
1.30	06.08	00.00
1.35	00.00	00.00
1.40	05.36	00.00
1.45	04.60	00.00
1.50	00.00	00.00
1.55	00.00	00.00
1.60	00.00	00.00
1.65	00.00	00.00
1.70	00.00	00.00
1.75	00.00	00.00
1.80	04.43	00.00
1.85	04.43	00.00
1.90	00.00	00.00
1.95	04.17	00.00
2.00	04.60	00.00
2.05	03.56	00.00

Table 6.4b

CSD Data for Quartzites from Lunavada region (Samples Q3 and Q4)

Size L (mm)	ln(n) Sample Q3	ln(n) Sample Q4
0.025	14.23	14.80
0.050	14.32	14.94
0.075	14.08	14.51
0.10	13.66	13.82
0.125	13.20	13.36
0.150	13.05	12.87
0.175	12.75	12.21
0.200	12.13	11.81
0.225	11.80	11.45
0.250	11.71	11.00
0.275	11.19	10.72
0.300	10.74	10.40
0.325	09.88	10.03
0.350	09.46	09.73
0.375	09.58	09.23
0.400	09.63	07.75
0.425	09.22	08.33
0.450	08.59	08.33
0.475	08.99	07.50
0.500	09.09	08.46
0.525	08.53	07.98
0.550	06.51	06.94
0.575	00.00	07.38
0.600	05.91	06.34
0.625	05.91	00.00

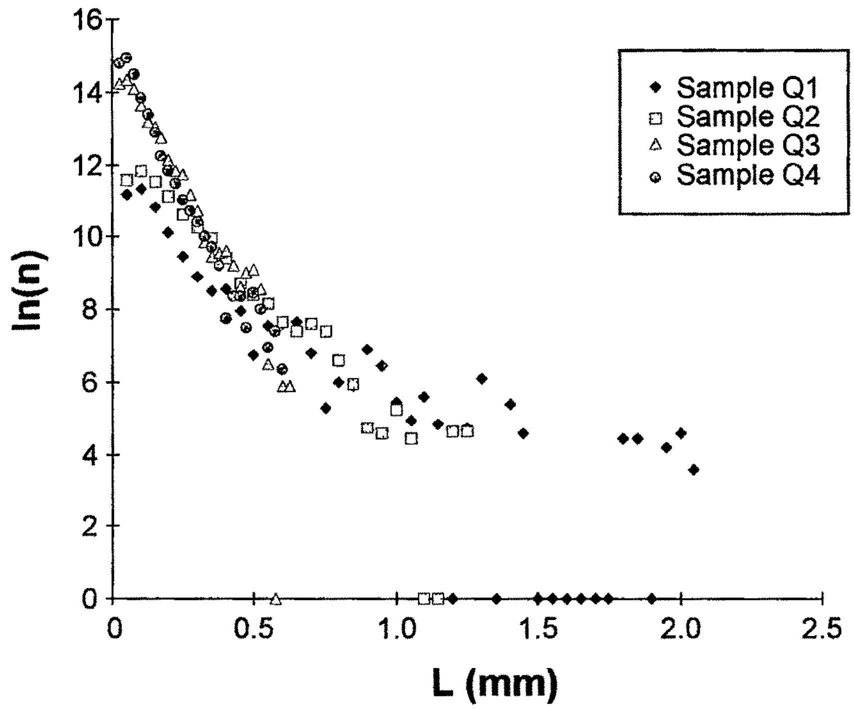

Fig. 6.24 CSD plot for quartzites

6.9. TIME RELATIONSHIP BETWEEN CRYSTALLIZATION AND DEFORMATION

The mica schists of the area around Lunavada and Santrampur contain several porphyroblasts of garnet and biotite which include foliations in the form of quartz inclusions trails. These schists also posses foliations of different generations as well as porphyroblasts with inclusion patterns. Because of these facts, the garnet biotite schists are ideal to understand the time relationship between crystallization and deformation.

Zwart (1962) was the first to use porphyroblast-matrix relations to propose criteria for determining the time relationship between crystallization and deformation. He defined the foliation included within the porphyroblasts in the form of inclusion trails was defined as S_i while the foliation outside was defined as S_e, and the S_i-S_e relationship was used to identify porphyroblasts as pre-, syn- and post-tectonic with respect to a particular foliation (Zwart, 1962). The criterion of different S_i-S_e relationships described by Zwart(1962) shown in Fig. 6.25 has been widely accepted to determine the timing of porphyroblast growth (Spry, 1969; Vernon, 1976; Ghosh 1993). Further expanding Zwart's classification, Passchier and Trouw (1996) proposed a four-fold classification of porphyroblasts as pre-, inter-, syn- and post-tectonic on the basis of porphyroblast matrix relationship (i.e. S_i-S_e relationships). They have added a new category 'inter-tectonic porphyroblasts' which are characterized by inclusion trails having no obvious continuity with the matrix foliation. Recently, Mamtani and Karanth (1996 c) proposed a criterion to distinguish syndeformational (syn-tectonic) from postdeformational (post-tectonic) porphyroblasts. They observed that inclusions of quartz in syn- and post- tectonic

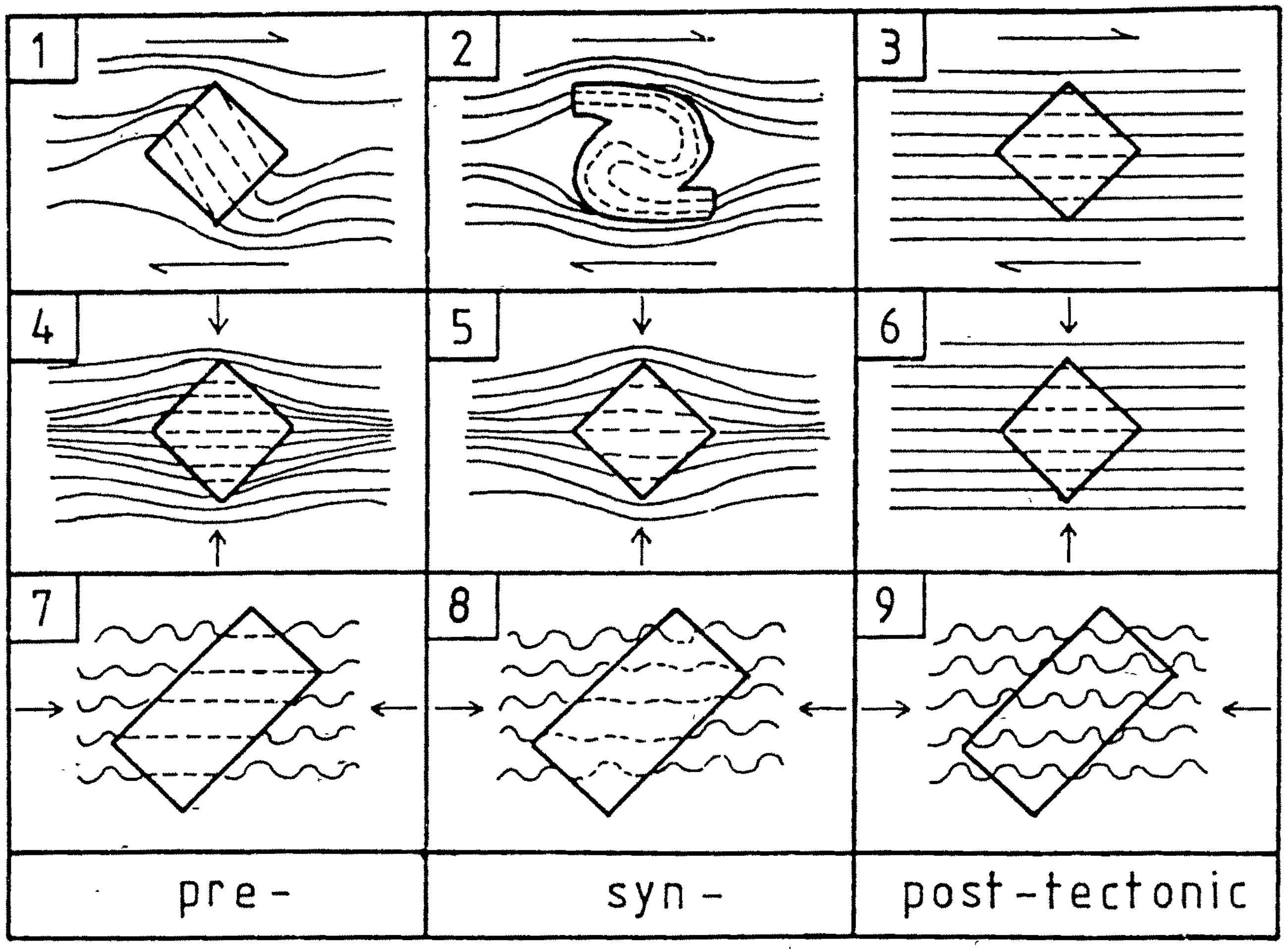

Fig 6.25 Diagram showing the "nine diagnostic forms" of porphyroblast-matrix relationships. The dashed lines represent inclusion trails (Si) while the continuous lines represent the external schistosity (Se). (After Zwart, 1962)

porphyroblasts have undulose and sharp extinction respectively. (Mamtani and Karanth, 1996 c). Fig. 6.26 explains the reason for the preservation of different types of extinction in syndeformational and postdeformational porphyroblasts. Accordingly, during deformation the quartz crystals in a pelitic rock respond to the external stresses by deformation of the lattice. This is manifested in the undulose extinction of quartz (Spry, 1969; White, 1973; Vernon, 1976) and if a porphyroblast grows simultaneously with deformation, it would include quartz grains with undulose extinction (Fig. 6.26, path A). But if the growth of a porphyroblast occurs due to a post deformational event, on account of heat outlasting deformation, the heat causes static recrystallization of the quartz grain, thus resulting in readjustment of the crystal lattice. Hence, earlier crystals with undulose extinction would recrystallize to a strain free state with sharp extinction due to heat outlasting the deformation. These quartz grains would then get included in the postdeformational porphyroblasts (Fig. 6.26, path B). Quartz can undergo syntectonic recrystallization under greenschists facies conditions (White, 1973, 1977; Ghosh, 1985) and this could result in destruction of undulose extinction from quartz inclusions in syntectonic porphyroblasts. However, according to Mamtani and Karanth (1996 c), a careful observation of such quartz inclusions under higher magnification in several syntectonic porphyroblasts has revealed that in such a situation undulose extinction is not totally destroyed and the same is preserved in some, if not all of the quartz inclusions.

The above criteria of Zwart (1962), Passchier and Trouw (1996) and Mamtani and Karanth (1996 c) were used by the present author as a basis to understand the porphyroblast-matrix relationships and determine the timing of porphyroblast growth in the schists of the area around Lunavada and Santrampur. Most of the garnet and

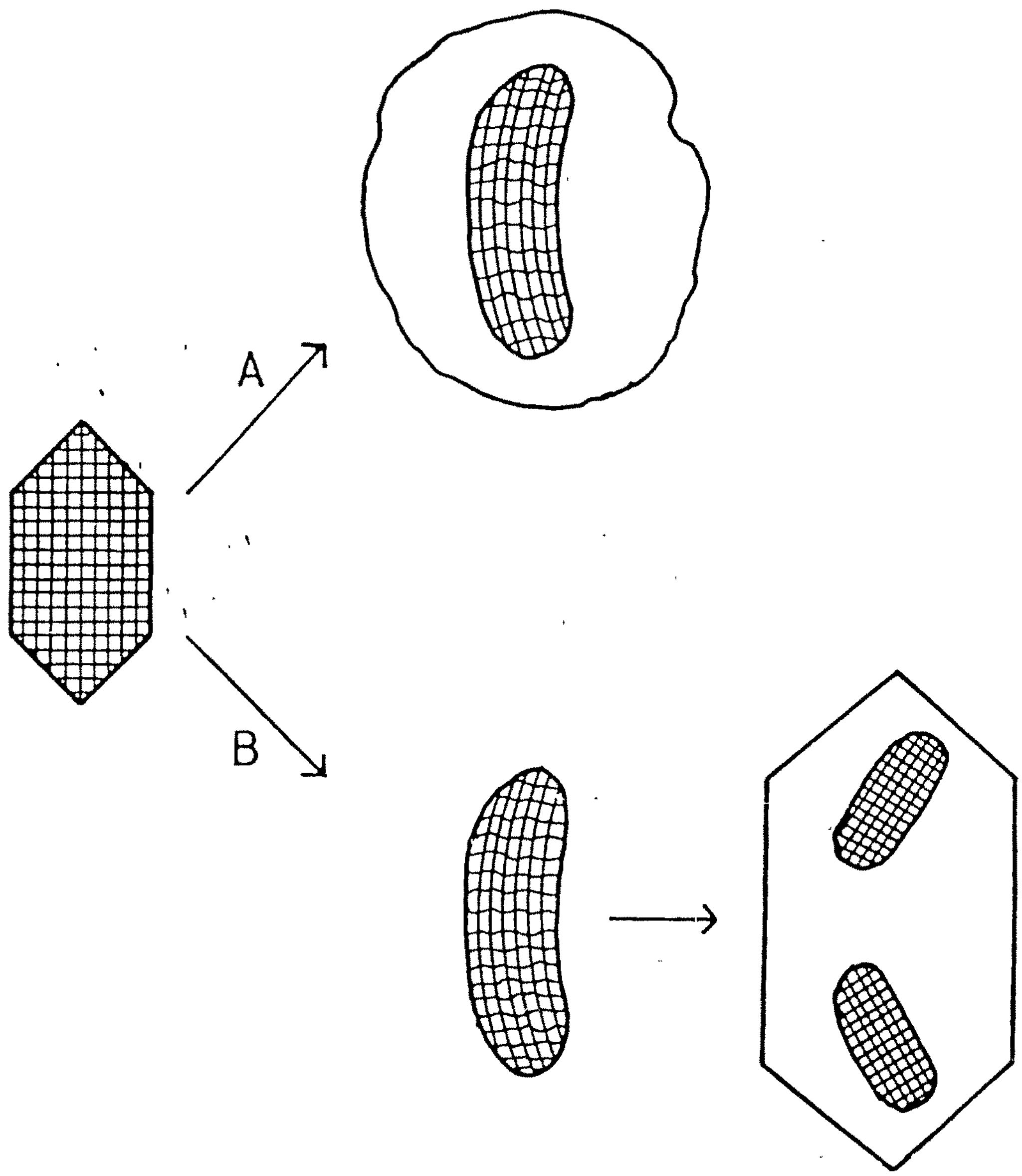

Fig 6 26 Schematic diagram representing the inclusion of quartz in syndeformational and postdeformational porphyroblasts. The grid simulates crystal lattice. An undeformed quartz crystal with a perfect crystal lattice is subjected to deformation. Along Path A, the growth of the porphyroblast occurs simultaneously with deformation and includes the quartz grain in the deformed state with an irregular (deformed) lattice. Hence, syndeformational porphyroblasts possess quartz inclusions showing undulose extinction. Along Path B, the porphyroblast grows due to postdeformational thermal event. This results in static recrystallization of the quartz grain and in readjustment of the lattice Therefore, the inclusions in postdeformational porphyroblasts have sharp extinction.(Fig is after Mamtani and Karanth, 1996c) biotite porphyroblasts preserving the microfolded or sigmoidal inclusion trails are identified as syntectonic with D_2 deformation (Figs. 6.9). A few garnet porphyroblasts have overgrown the crenulation cleavage (S_2) (Fig. 6.10). Such porphyroblasts preserve sigmoidal inclusion trails of quartz and feldspar ($S_1 = S_i$) which gradually curve into S_2 within the porphyroblast. On the other hand the cleavage domain outside the porphyroblast has only a single schistosity S_2 (Figs.6.10, 6.27). Such porphyroblasts are identified as syndeformational (syn-tectonic) with D_2 deformation. The stages of growth which the above porphyroblast in Fig. 6.10 (and 6.27) might have undergone are shown in Fig. 6.28.

In Fig. 6.28, it will be seen that the porphyroblast has overgrown the differentiated crenulation cleavage syntectonically during stage 4a of crenulation cleavage genesis given by Mamtani and Karanth (1996a; please refer to Section 6.6 for details), thus preserving S_1 inclusion trails curving sigmoidally into S_2 within the porphyroblast. Due to continuing deformation, the matrix foliation further deforms and rotates into parallelism with the S_2 while the sigmoidal relation between S_1 and S_2 within the porphyroblast remains frozen in the same stage at which it was included, thus remaining unaffected by later deformation. Some of the inclusions also show undulose extinction. Therefore the porphyroblast in Fig. 6.10 which has overgrown the crenulation cleavage can be considered as syntectonic with the formation of crenulation cleavage S_2 i.e., syn-D_2 . Bell et. al. (1986, 1992) and Bell and Hayward (1991) have suggested that a porphyroblast cannot overgrow a crenulation cleavage syntectonically during the same deformation event which resulted in the development of the crenulation cleavage because shear assisted dissolution would disallow such a growth. Passchier et. al. (1992) have contradicted

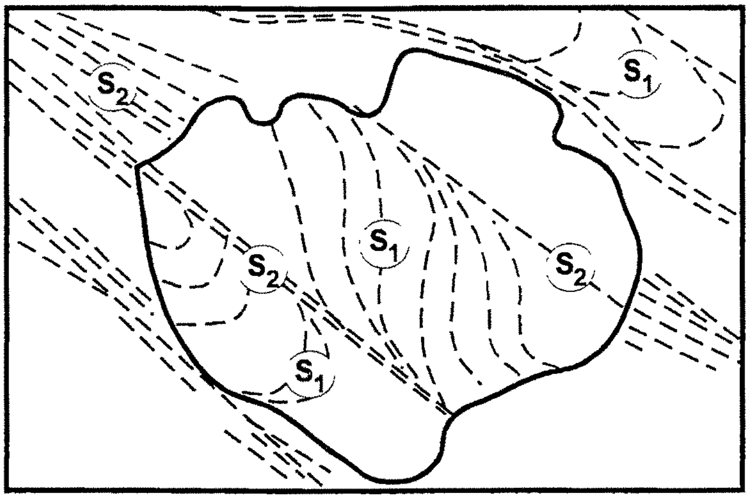

Fig. 6.27. Explanatory line drawing of microstructural relationships observed in Fig. 6.10b. The garnet has grown over the crenulation cleavage zone (S2) during D2 deformation. The S1 inclusion trails curve sygmoidally into S2 within the porphyroblast whereas the cleavage zone has a single schistosity (S2).

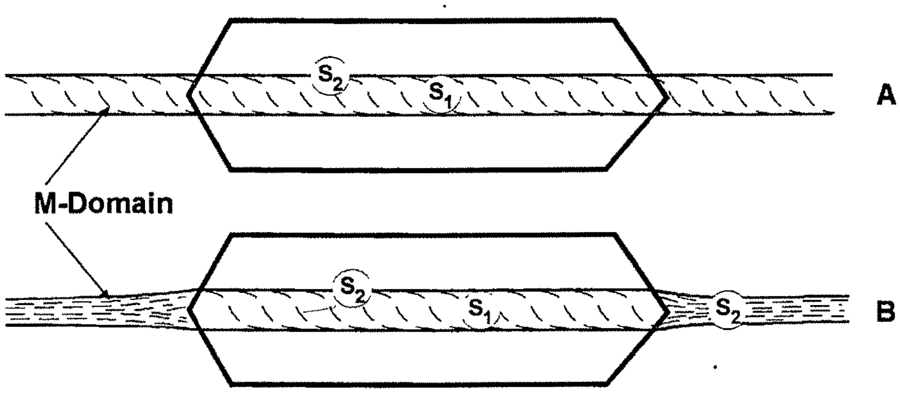

Fig. 6.28. Schematic diagram simulating stages of growth of a porphyroblast over crenulation cleavage during crenulation cleavage genesis. In stage A, the porphyroblast overgrows crenulation cleavage (M-domain) to include S1 inclusion trails sigmoidally curving into S2 within the porphyroblast. Similar relationship exists in the cleavage zone (M domain) outside the porphyroblast. Due to continued deformation the S1 in the M domain outside the porphyroblast has totally rotated into parallelism with S2 in stage B. The S1 inclusion trails within the porphyroblast maintain the same orientation as in stage A. (after Mamtani and Karanth, 1997).

this by providing evidences of porphyroblasts overgrowing the cleavage zones *(Fig. 8-10 in Passchier et.al.1992)*, which they consider as synkinematic with crenulation cleavage genesis. Similar evidences have also been provided by Gururajan (1994) The above Fig. 6.10 supports the interpretations of Passchier et al. (1992) and Gururajan (1994) that porphyroblasts can indeed overgrow crenulation cleavages syntectonically during the same episode of deformation which resulted in the formation of the crenulation cleavage.

As mentioned in the Section 6.3 it is known that chlorite and biotite crystals of more than one generation are present. Chlorite(1) and Biotite(1) occur along the S_1 schistosity and are syn-D_1. The metamorphic event which accompanied D_1 is referred to as M_1 . Biotite(2) crystals which occurs with their (001) planes parallel to S_2 have grown during D_2 deformation. Biotite(2) porphyroblasts with spiral (helictic) inclusions trails of quartz (e.g. Fig. 6.9) are also syn-D_2. Similarly the garnet porphyroblasts with helictic inclusion trails of quartz (e.g. Fig. 6.10) and those with inclusion trails oblique to external schistosity (e.g. Fig. 6.8) are also syn-D_2. The metamorphic event which accompanied D_2 deformation is referred to as M_{2-1}. M_1 and M_{2-1} events were progressive. These were followed by retrogressive metamorphism (M_{2-2} during the waning phases of D_2 deformation. The last metamorphic event to affect the rock was a syn/post-D_3 thermal event which caused some static recrystallization of muscovite and quartz. Fig. 6.29 summarizes the time relationship between crystallization and deformation of various minerals in garnet mica schists.

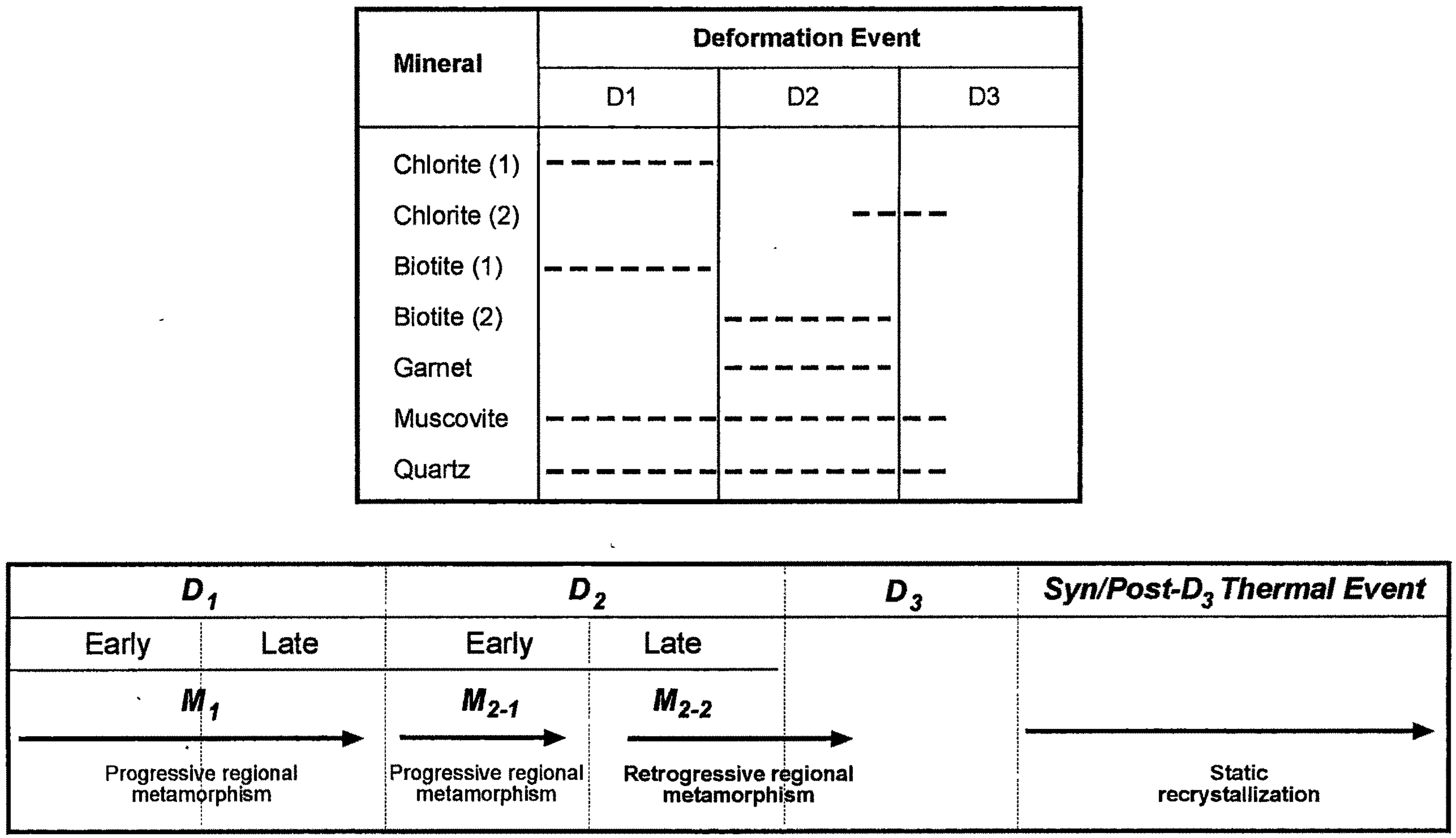

Fig. 6.29. Diagram showing the time relationship between crystallization and deformation in garnet mica schists of the Lunavada region.